



Chapter X

The La Pitarrilla Silver-Zinc-Lead Deposit, Sierra Madre Occidental, Mexico: A Description of the Mineralization and a Reconstruction of Its Volcano-Sedimentary Environment

CLAIRE M. J. SOMERS,^{1,†} HAROLD L. GIBSON,¹ AND RON BURK²

¹*Mineral Exploration Research Centre, Department of Earth Sciences, Laurentian University, 935 Ramsey Lake Road, Sudbury, Ontario, Canada P3E2C6*

²*Silver Standard Resources Inc., 999 West Hastings Street, Suite 1400, Vancouver, British Columbia, Canada V6C2W2*

Abstract

The La Pitarrilla Ag-Zn-Pb deposit, Mexico, is hosted by Cretaceous, Eocene, and Oligocene strata that record a complex volcano-sedimentary, structural, and hydrothermal history. Deformed Cretaceous rocks form the basement to unconformably overlying Eocene and Oligocene volcanic strata. The Eocene volcanoclastic strata were derived from arc volcanism and from the erosion of subaerial arc volcanoes, with the clastic material transported by sedimentary gravity flows and deposited into a below storm wave base basin that developed within a back-arc extensional setting. Uplift of the arc during the Eocene was accompanied by extension and voluminous silicic pyroclastic volcanism, which is manifested by ignimbrite and pyroclastic surge deposits dated at 49.8 ± 1.0 Ma. Erosion during the Eocene and early Oligocene was accompanied or followed by northeast- and north-northwest-trending faulting, the emplacement of rhyolitic and andesitic sills and dikes, and a 31.59 ± 0.52 Ma rhyolitic dome.

The La Pitarrilla Ag-Zn-Pb deposit is characterized by iron oxide- and sulfide-associated mineralization, which defines a vertically stacked mineralized system centered on rhyolitic dikes and sills that constitute the feeder system for an early Oligocene volcanic center manifest by a rhyolitic dome. The sulfide-associated mineralization is rooted in the basement Cretaceous sedimentary strata and is represented by an areally restricted but vertically extensive zone of disseminated and vein-hosted Ag-Zn-Pb (-Cu-As-Sb) sulfide mineralization and strata-bound replacement mineralization within conglomerates that occur at the Cretaceous-Eocene unconformity. The sulfide mineralization extends upward into the overlying Eocene and Oligocene volcanoclastic strata and rhyolitic sills, where it abruptly grades into a laterally more extensive, supergene zone of disseminated iron oxide-associated mineralization that replaced the sulfides. The main Ag-Zn-Pb mineralization event is interpreted to have occurred during or after emplacement of the early Oligocene rhyolitic dome.

Introduction

THE LA PITARRILLA Ag-Zn-Pb deposit, owned by Silver Standard Resources Inc., is located in the north-central Durango State, Mexico, approximately 175 km north-northwest of the city of Durango and within the eastern flank of the central sector of the Sierra Madre Occidental mountain range (Fig. 1). The deposit is situated between the major silver mining centers of San Francisco del Oro-Santa Barbara and Fresnillo, which occur along the axis of the north-northwest-trending Mexican silver belt that extends from southern Chihuahua State to Mexico State (Damon et al., 1981; Camprubí et al., 2003; Camprubí and Albinson, 2007). Most epithermal precious and base metal deposits within the Mexican silver belt display characteristic features of both low- and intermediate-sulfidation epithermal deposits (Sillitoe and Hedenquist, 2003) and are associated with calc-alkaline arc magmatism (Damon et al., 1981) and postsubduction extension (Camprubí and Albinson, 2007).

The mineral potential at La Pitarrilla was first recognized in October 1995 by La Cuesta International as part of a generative gold exploration program for Monarch Resources Ltd. Between December 1995 and June 1998, Monarch completed

extensive soil, rock-chip, and stream-sediment sampling programs, and drilled 22 reverse-circulation boreholes to test gold geochemical anomalies that had been identified. Because assay results were not encouraging, Monarch signed over the concession titles to La Cuesta International in mid-1998. As a result of the mining industry recession in 2000, La Cuesta International abandoned the La Pitarrilla mineral concessions in 2001. In May 2002, La Cuesta International entered into an agreement with Silver Standard Resources Inc. to conduct generative silver exploration in Mexico. One of the first recommendations of La Cuesta International was to reclaim the La Pitarrilla property, which took place in June 2002.

La Cuesta International prospected the reclaimed concessions in July 2002 to search for the source of Ag-Pb-Zn stream-sediment anomalies that had previously been identified in seasonal drainages on the slopes of the Cerro La Pitarrilla. New rock-chip samples collected from flow-banded rhyolite on the western flank of the peak yielded silver assay values as high as 220 g/t Ag together with anomalous concentrations of Zn, Pb, Sb, and Hg. In the following months, an exploration team lead by Guillermo Lozano carried out extensive rock-chip sampling and geologic mapping, which was followed by a program of reverse-circulation drilling. In

[†] Corresponding author: e-mail, cm_somers@laurentian.ca

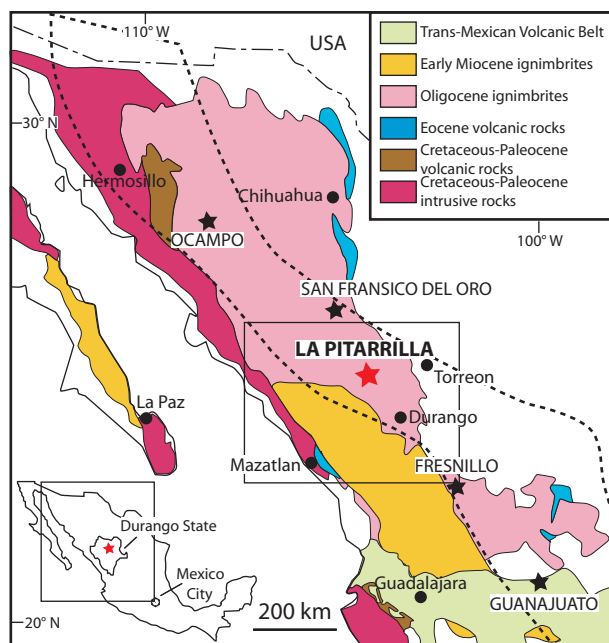


FIG. 1. Distribution of the Sierra Madre Occidental igneous complexes (after Ferrari et al., 2007), showing the location of the central sector of the Sierra Madre Occidental (dark square), the Durango State, the La Pitarrilla Ag-Zn-Pb deposit (red star), and other important Mexican epithermal precious and base metal deposits (red and dark stars), which occur along the axis of a north-northwest-trending Mexican silver belt (dashed line; after Camprubí and Albinson, 2007).

October 2003, Silver Standard Resources Inc. announced the discovery of the Cordon Colorado mineralized zone, where one of the early drill holes had intersected 63 m of oxidized, disseminated mineralization averaging 173 g/t Ag. In the six years following the discovery, Silver Standard Resources Inc. drilled 186 reverse-circulation and 365 diamond drill holes for a total of 199,658 m to outline the five zones of Ag-Zn-Pb mineralization that today constitute the La Pitarrilla deposit. In August 2008, the company reported measured and indicated mineral resources of 236 million metric tons (Mt).

The present study provides the first description of the geology and mineralization at the La Pitarrilla Ag-Zn-Pb deposit and one of the first detailed and comprehensive descriptions of the Eocene volcanic strata and their depositional environments within the Sierra Madre Occidental. The primary objectives of this research were to (1) describe the Ag-Zn-Pb mineralization styles at La Pitarrilla; (2) reconstruct the volcano-sedimentary and tectonic history of the Tertiary strata that host the mineralization, thereby providing a new understanding of the timing and environment(s) of the mineralization; and (3) describe the primary stratigraphic, structural, and volcanic controls on mineralization. The results presented herein contribute to the understanding of the genesis of the Mexican epithermal silver deposits and may aid future exploration in the Mexican silver belt.

Regional Geology and Tectonics

The Sierra Madre Occidental volcanic province has a minimum estimated volume of 400,000 km³, varies in width from 250 to 600 km, and extends over 1,000 km from the United

States-Mexico border southward to its intersection with the Trans-Mexican volcanic belt (Aguirre-Díaz and Labarthe-Hernández, 2003; Aguirre-Díaz et al., 2008; Fig. 1). The Sierra Madre Occidental is the erosional remnant of a north-northwest-trending, calc-alkaline magmatic arc that formed during the Eocene to early Miocene in response to subduction of the Farallon plate beneath North America (Ferrari et al., 1999). During the early to middle Miocene, the southern part of the arc was reoriented to an east-west direction, which is represented by the Trans-Mexican volcanic belt (Ferrari et al., 1999; Fig. 1).

The La Pitarrilla Ag-Zn-Pb deposit is located within the eastern flank of the central sector of the Sierra Madre Occidental, where the basement consists of Mesozoic marine sedimentary rocks that were deformed during the Laramide orogeny and are interpreted to belong to the Mezcalera Formation (Munguía-Rojas et al., 2000; Dromundo-Arias and Peral-Carranza, 2007); micro- and macro-fossils indicate ages ranging from Neocomian to Cenomanian-Turonian (Araujo-Mendieta and Arenas-Partida, 1986). The Mesozoic sedimentary succession consists of argillaceous limestone, mudstone, siltstone, sandstone, and heterolithic conglomerate composed of volcanic and sedimentary rock clasts (Araujo-Mendieta and Arenas-Partida, 1986; Dickinson and Lawton, 2001; Franco-Rubio et al., 2007).

The lower volcanic complex, as originally defined by McDowell and Clabaugh (1979), unconformably overlies the Mesozoic sedimentary basement and consists of 52 to 40 Ma dacitic-andesitic flows and domes, and lesser silicic domes and ignimbrites, which were interpreted to be the products of continental arc volcanism (Aguirre-Díaz and McDowell, 1991; Ferrari et al., 2007; Aguirre-Díaz et al., 2008). The Eocene volcanic strata are commonly underlain and rarely overlain by reddish conglomerates, sandstones, and mudstones (McDowell and Clabaugh, 1979; Aranda-Gómez and McDowell, 1998; Horner and Enriquez, 1999) that contain andesitic volcanic and Mesozoic sedimentary rock clasts (Aguirre-Díaz and McDowell, 1991; Nieto-Samaniego et al., 1999; De La Garza et al., 2001). In this paper, the calc-alkaline volcanic strata and clastic sedimentary rocks are grouped into one package of volcanic rocks, referred to as the Lower Volcanic Succession, as it undoubtedly consists of more than one volcanic complex.

The upper volcanic supergroup of McDowell and Keizer (1977), also referred to as the ignimbrite flare-up (Ferrari et al., 2007; Aguirre-Díaz et al., 2008), unconformably overlies the Lower Volcanic Succession and consists of a thick succession of voluminous silicic ignimbrite, rhyolitic domes, and minor basaltic to andesitic lavas (Ferrari et al., 2002, 2007; Aguirre-Díaz et al., 2008) that were extruded in the central sector of the Sierra Madre Occidental from 32 to 29 Ma (Aguirre-Díaz and Labarthe-Hernández, 2003) and from 24 to 20 Ma (Ferrari et al., 2002, 2007). The term Upper Volcanic Succession is used here to be consistent with the stratigraphic nomenclature introduced above. Basaltic-andesitic volcanism appears to have followed each major ignimbritic episode (Ferrari et al., 2007) and locally covers the Oligocene Upper Volcanic Succession (Aguirre-Díaz and McDowell, 1993; Luhr et al., 2001).

From a structural perspective, the relatively unfaulted Sierra Madre Occidental separates two north-northwest-trending

regions, the Chihuahua and Mexican Altiplano region to the east and the Gulf of California region to the west, which contains extensional structures, such as grabens and half-grabens, horsts, and tilted blocks (Henry and Aranda-Gómez, 1992; Stewart, 1998). The eastern flank of the central sector of the Sierra Madre Occidental, where the La Pitarrilla deposit is located, has been interpreted to have undergone two major periods of extension. The first extension, directed east-northeast–west-southwest, occurred from 32.3 to 30.6 Ma, at about the same time as the main episode of ignimbritic volcanism recorded by the Upper Volcanic Succession (Aguirre-Díaz and McDowell, 1993; Luhr et al., 2001). The second extension, directed east-northeast, postdated Oligocene silicic volcanism (ca. 24 Ma) but coincided with a mafic, alkaline volcanic event (Aguirre-Díaz and McDowell, 1993; Luhr et al., 2001).

Geology of the La Pitarrilla Deposit

Stratigraphy and lithofacies

Detailed mapping at a scale of 1:1000 and relogging of approximately 28,000 m of drill core allowed a subdivision of the La Pitarrilla stratigraphy into informal formations, members, and lithofacies in accordance with the North American Stratigraphic Code (North American Commission on Stratigraphic Nomenclature, 2005). Four informal formations were recognized which, from oldest to youngest, are the Peña Ranch, Pitarrilla, Cardenas, and Casas Blancas formations (Figs. 2–5). A detailed description and interpretation of each member, their contained lithofacies, as well as definitions regarding nomenclature and terminology used herein are given in the Appendix.

The Peña Ranch formation forms the Cretaceous basement to Eocene and Oligocene volcanic strata and was folded during the Laramide orogeny (Figs. 2–5). This formation is dominated by interbedded low-density turbidity current deposits with lesser gravelly high-density turbidity current deposits and micritic limestone that were deposited below storm wave base and within a marine environment. The Peña Ranch formation is interpreted to be the stratigraphic equivalent of the Cretaceous Mezcalera Formation (Fig. 2).

The Pitarrilla formation unconformably overlies the Peña Ranch formation and consists of the Manto Rico, Lower, Middle, and Upper members that were emplaced in a below storm wave base marine environment (Figs. 2–5). The Manto Rico member, located at the Cretaceous-Eocene unconformity, consists of channelized, limestone clast-bearing conglomerates that also contain clasts of terrigenous sedimentary rocks, and andesitic clasts identical to those of the overlying Lower member. The Manto Rico member is the most economically important ore host at the La Pitarrilla deposit. The Lower to Upper members consist of multiple cohesive debris flow deposits interbedded with low- and high-density turbidity current deposits and a single andesitic flow that has an arc affinity. The particulate gravity flows of the Lower to Upper members are dominantly composed of dacitic and andesitic clasts that were derived from unconsolidated subaerial or subaqueous volcanoclastic deposits or flows with a calc-alkaline arc signature, except for the limestone clasts and the clasts of terrigenous sedimentary rocks that were derived

from the underlying Peña Ranch formation or equivalent units.

The Cardenas formation unconformably overlies the Pitarrilla formation and consists of the lithic-rich tuff and lapilli tuff lithofacies, the crystal-rich pumice tuff lithofacies, the stratified tuff lithofacies, and the lithic-rich tuff lithofacies (Figs. 2–5). The lithic-rich tuff and lapilli tuff lithofacies and the lithic-rich tuff lithofacies contain lithic sedimentary and volcanic clasts and clay-altered, wispy clasts that define a planar fabric within depositional units. The wispy clasts resemble pumice and these lithofacies may represent incipiently welded or nonwelded ignimbrites. The crystal-rich pumice tuff lithofacies consists of the crystal- and pumice-rich tuff facies and the stratified facies. The crystal- and pumice-rich tuff facies contains clay-altered, flattened, and wispy quartz and K-feldspar porphyritic, long-tube pumice clasts, and lesser lithic volcanic and sedimentary clasts. The pumice clasts define a pronounced eutaxitic texture that is interpreted to have formed during welding and compaction. The stratified facies is a planar and cross-stratified tuff. Columnar joints within both facies indicate hot deposition, and they are interpreted as welded ignimbritic and pyroclastic surge deposits, respectively, which were emplaced in a subaerial environment. The overlying stratified tuff lithofacies consists of planar beds and is interpreted as a high-density turbidity current deposit that was emplaced within a subaqueous environment (lacustrine or marine).

The Casas Blancas formation unconformably overlies tilted strata of the Cardenas formation and consists of a lower and upper volcanoclastic lithofacies, and an overlying coherent rhyolitic lithofacies referred to as the Encino rhyolitic dome (Figs. 2–5). Both the upper and lower volcanoclastic lithofacies are dominantly composed of andesitic and dacitic clasts, but the upper volcanoclastic lithofacies also contains clasts of the Encino rhyolitic dome. The conformably overlying massive and flow-banded Encino rhyolitic dome contains hyaloclastite along its basal contact and is interpreted to have been emplaced in whole or in part in a subaqueous environment (lacustrine or marine) or onto wet and unconsolidated volcanoclastic rocks.

Two mafic sills occur within the volcanoclastic succession. The lower mafic sill is located at the base of the Pitarrilla formation and its emplacement is interpreted to be postfaulting but pre-Encino rhyolitic dome emplacement (Figs. 2–5). The upper mafic sill is located at the base of the Casas Blancas formation and it was emplaced during or just after emplacement and growth of the Encino rhyolitic dome (Figs. 2–5). The sills are andesitic in composition and have an arc affinity. A localized swarm of northeast-southwest and north-northwest–south-southeast felsic dikes and sills crosscut all formations, except for the Encino dome as the felsic intrusions are interpreted to be the feeders for the Encino dome (Figs. 2–5). The felsic intrusions and Encino rhyolitic dome are identical in composition, and, unlike the mafic sills, their compositions are not typical of an arc affinity (App.).

Geochronology

To place the lithofacies and formations at La Pitarrilla in the context of the stratigraphy of the Sierra Madre Occidental, two samples were collected for U-Pb age determination

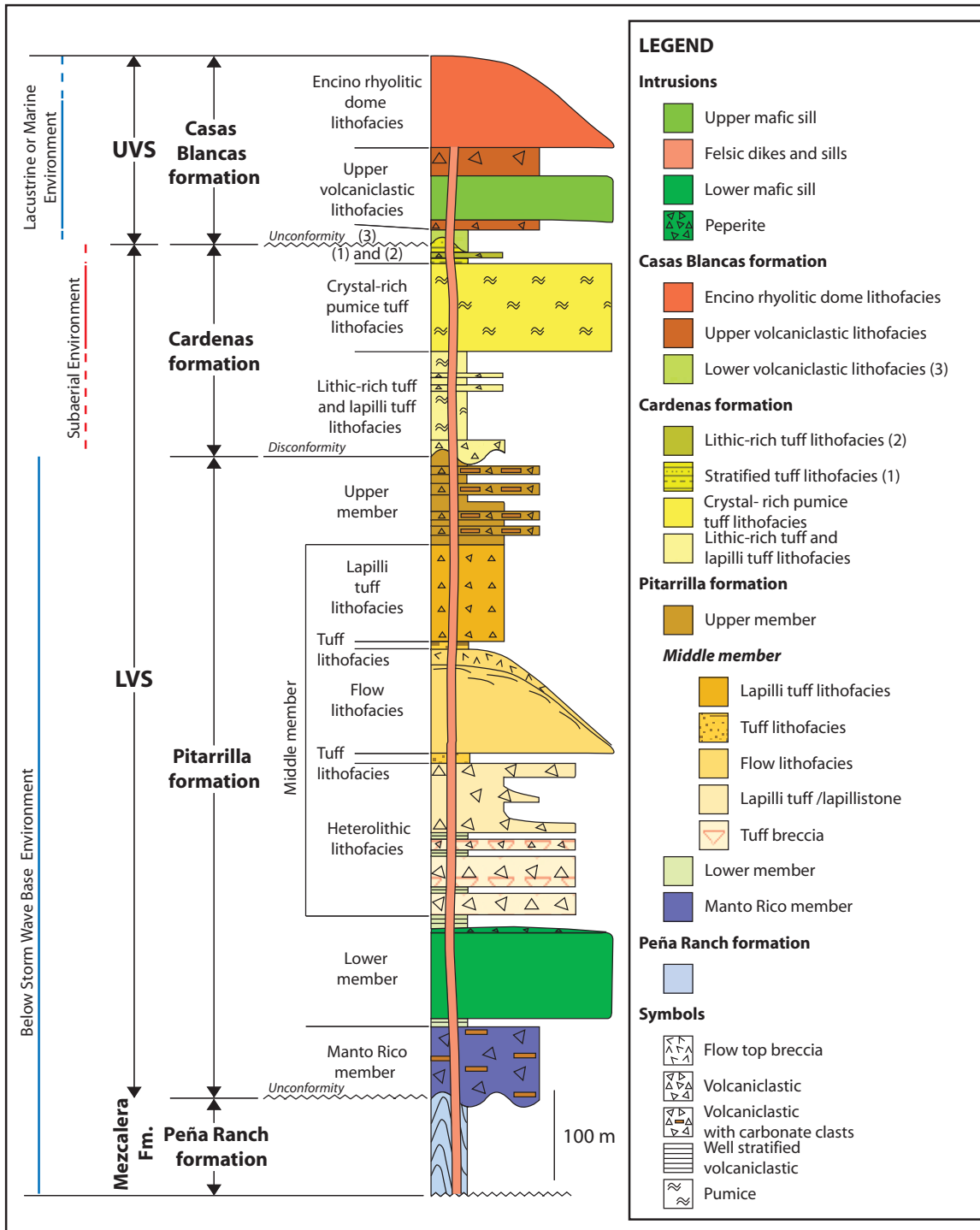


FIG. 2. Idealized stratigraphic section through the La Pitarrilla deposit, showing the informal formations, members, lithofacies, their depositional environments, and their interpreted stratigraphic relationship to Sierra Madre Occidental stratigraphy (LVS = Lower Volcanic Succession; UVS = Upper Volcanic Succession).

on zircons. One sample is from the welded ignimbrite of the Cardenas formation, i.e., crystal- and pumice-rich tuff facies, and a second is from the Encino rhyolitic dome of the Casas Blancas formation.

The U-Pb age determination on zircons were performed at the Department of Earth Sciences, Laurentian University

(Sudbury, Ontario), using a laser ablation-inductively coupled-plasma mass spectrometer (LA-ICP-MS), consisting of a 213-nm Nd:YAG laser (NewWave) connected to a quadrupole ICP-MS (Thermo X Series II). Zircon grains were separated and cast in epoxy mounts or placed on double-sided sticky tape. The grains were ablated following the analytical

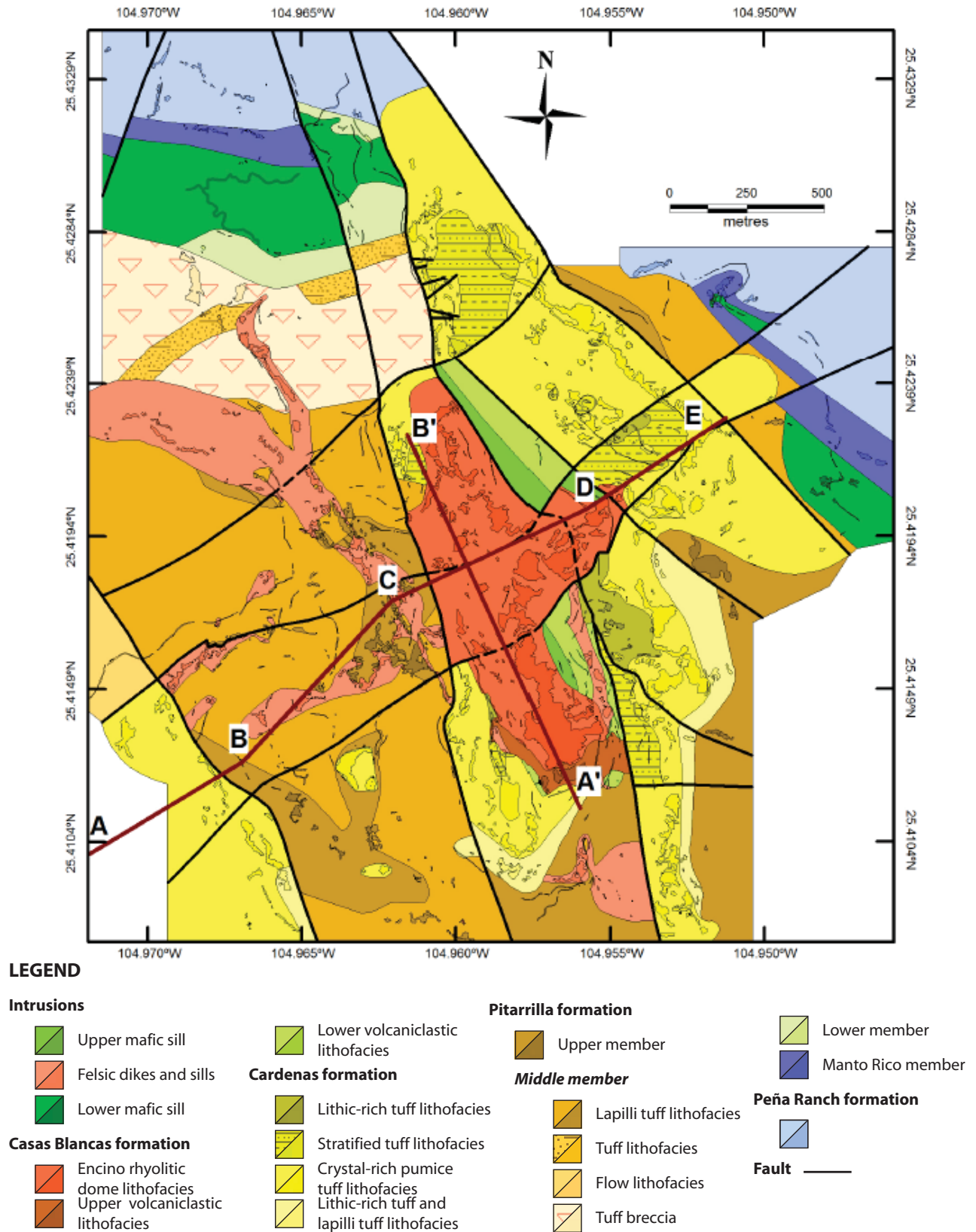


FIG. 3. Geologic map of the La Pitarrilla deposit and the location of two cross sections. Faults shown were activated and reactivated postemplacement of the Cardenas formation. Where the faults are represented by a dashed line, they are covered by the Encino rhyolitic dome lithofacies or crosscut by felsic intrusions.

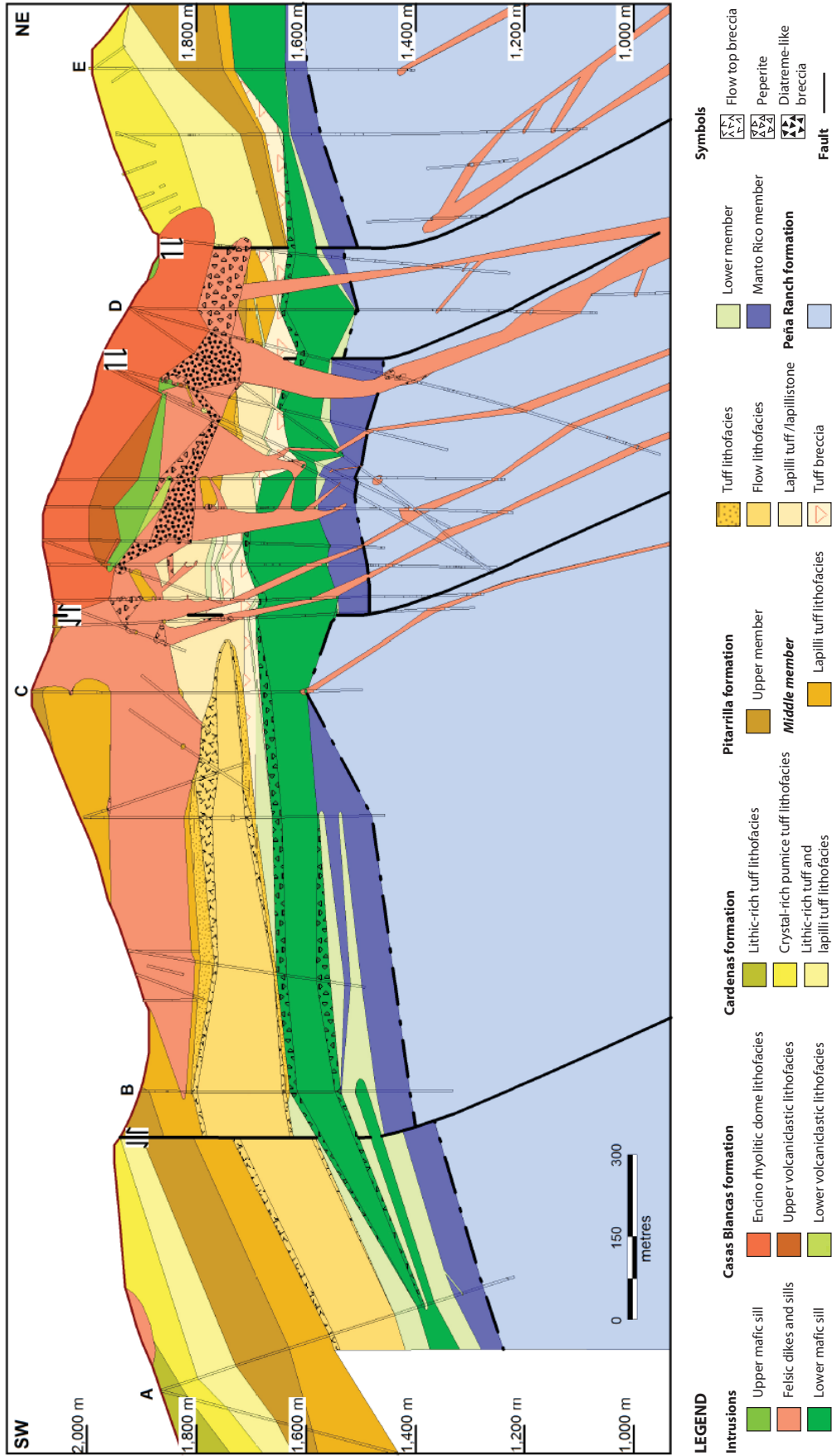


FIG. 4. A northeast-southwest geologic cross section through the La Pitarilla deposit (see Fig. 3 for the location of section), showing an erosional unconformity between the Peña Ranch and Pitarilla formations (dark dashed line). The diatreme-like breccias developed within the felsic dike complex are shown.

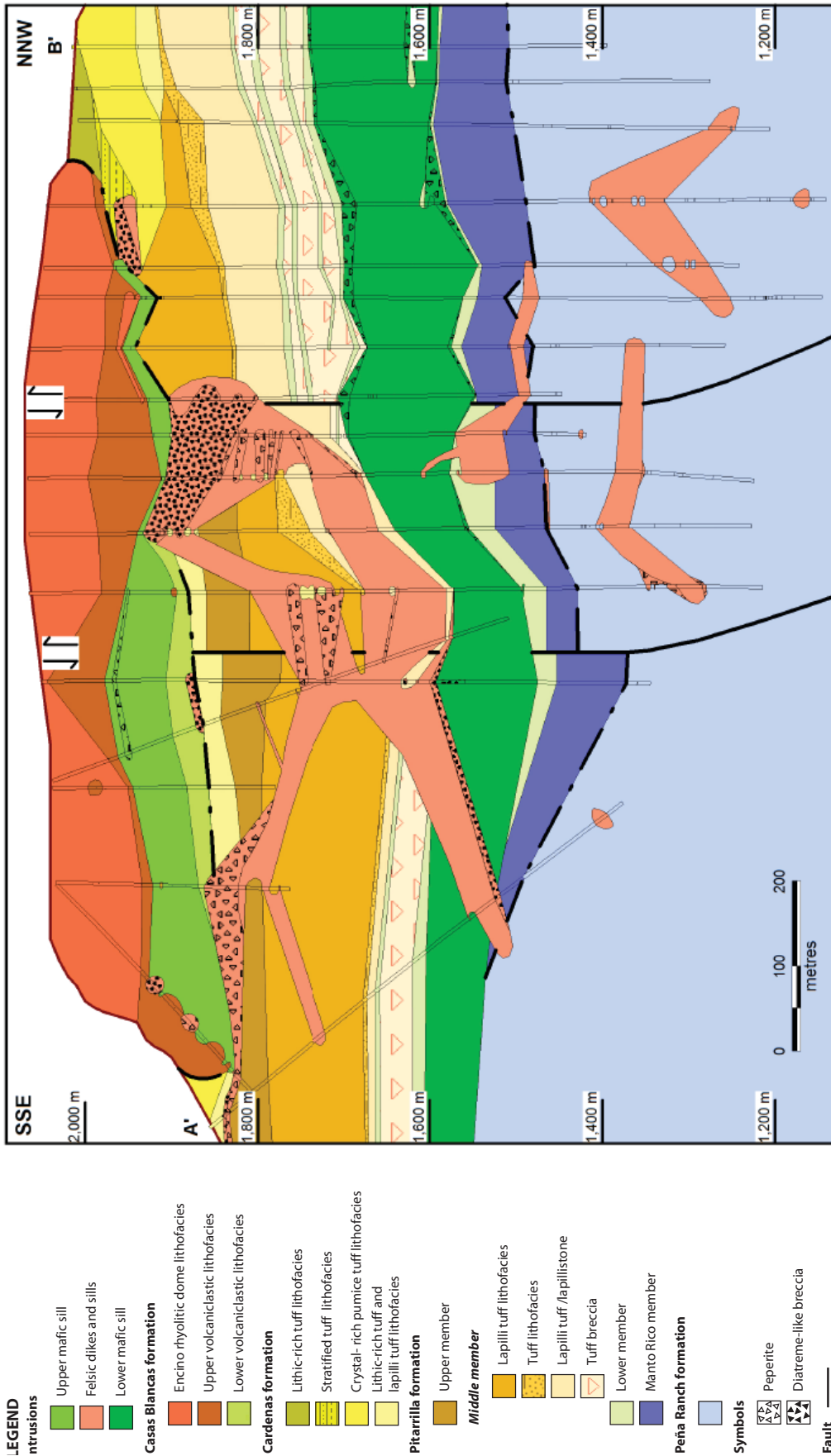


FIG. 5. A north-northwest-south-southeast geologic cross section through the La Pitarrilla deposit (see Fig. 3 for the location of section), showing the erosional unconformities between the Peña Ranch and Pitarrilla formations and between the Cardenas and Casas Blancas formations (dark dashed lines). The diatreme-like breccias developed within the felsic dike complex are shown.

procedure of Benn and Kamber (2009) and Ulrich et al. (2009). Geostandard zircon 91500 yielded an uncorrected $^{207}\text{Pb}/^{206}\text{Pb}$ age of 1065.4 ± 7.2 Ma, well within the established age range (Wiedenbeck et al., 1995; Yuan et al., 2004). Sample data were corrected for common Pb using the routine of Andersen (2002). Concordia diagrams were calculated using the Isoplot software of Ludwig (2003).

Zircon grains from the welded ignimbrite of the Cardenas formation yielded many concordant analyses and a linear array of apparent discordia toward an older upper intercept. This yields a tightly constrained younger intercept U-Pb age of 49.8 ± 1.0 Ma (MSWD = 0.78; Fig. 6A) and indicates that the Cardenas formation is of Eocene age. This age suggests that the Cardenas formation and the underlying Pitarrilla formation belong to the Lower Volcanic Succession. The new age is consistent with K/Ar ages of 51.5 Ma and 42.9 ± 2 Ma obtained from two ignimbrites, the Abasolo and Boquillas Coloradas tuffs, located approximately 30 and 90 km SE of La Pitarrilla (Aguirre-Díaz and McDowell, 1991).

Zircons from the Encino dome of the Casas Blancas formation yielded a concordia intercept U-Pb age of 31.59 ± 0.52 Ma (MSWD = 0.88; Fig. 6B) that indicates an Oligocene age for the Encino dome. The Casas Blancas formation, therefore, belongs to the Upper Volcanic Succession. This age is consistent with K/Ar ages of 30.9 ± 0.7 and 29.3 ± 0.6 Ma previously obtained from two felsic domes, the R-7 and R-10 domes, located approximately 40 km southeast of La Pitarrilla (Aguirre-Díaz and McDowell, 1991).

Structural history

A major erosional event is represented by a well-defined angular unconformity between folded Cretaceous sedimentary basement rocks, represented by the Peña Ranch formation, and the shallowly dipping Eocene Pitarrilla formation (Figs. 2, 4, 5). The unconformity is marked by conglomerates of the Manto Rico member.

Steeply dipping listric faults define the main structural event at La Pitarrilla. Two fault sets are recognized that

include northwest-dipping, northeast-trending faults, designated here as faults A to C, and east-dipping, north-northwest-trending faults, denoted as faults D to H (Fig. 7). The north-northwest-trending faults tilt the originally subhorizontal strata of the Pitarrilla and Cardenas formations by as much as 35° to the southwest (Fig. 4), whereas the northeast-trending faults tilt these same strata by as much as 28° to the south-southeast (Fig. 5). The fault surfaces are generally not exposed; however, offsets of 20 to 150 m of the shallowly dipping strata of the Pitarrilla and Cardenas formations along the inferred faults indicate normal and reverse dip-slip components of displacement (Figs. 4, 5). Horizontal slip components along the principle faults are generally minor or insignificant (Figs. 3, 7), although such displacements are observed along the northern end of fault E (sinistral) and along the eastern end of faults B (sinistral) and C (dextral). Minimal evidence of horizontal displacements between the two fault sets suggests that these faults could be contemporaneous; however, the lack of outcrops along the faults makes this interpretation tentative.

The relatively flat-lying Casas Blancas formation overlies the faulted and tilted Cardenas formation and its deposition appears to have postdated the faulting that tilted and displaced the older formations (Figs. 4, 5). However, the two north-northwest- and northeast-trending lobes of the overlying rhyolitic dome are laterally restricted by the vertically projected continuation or trace of these early faults, and the lobes themselves have trends that are broadly parallel to the orientation of the two fault sets (Figs. 3, 7). This suggests that fault-bounded topographic basins may have confined the emplacement or allowed parts of the rhyolitic dome, which filled these paleotopographic depressions, to be preserved from erosion. The felsic dikes, interpreted as feeders to the rhyolitic dome, also define two trends, a north-northwest and a northeast trend, which are parallel to the two fault sets described above (Figs. 3, 7). The more abundant north-northwest-trending dikes dip steeply to the northeast, similar to the north-northwest-trending faults (Figs. 4, 5). The common trends of the

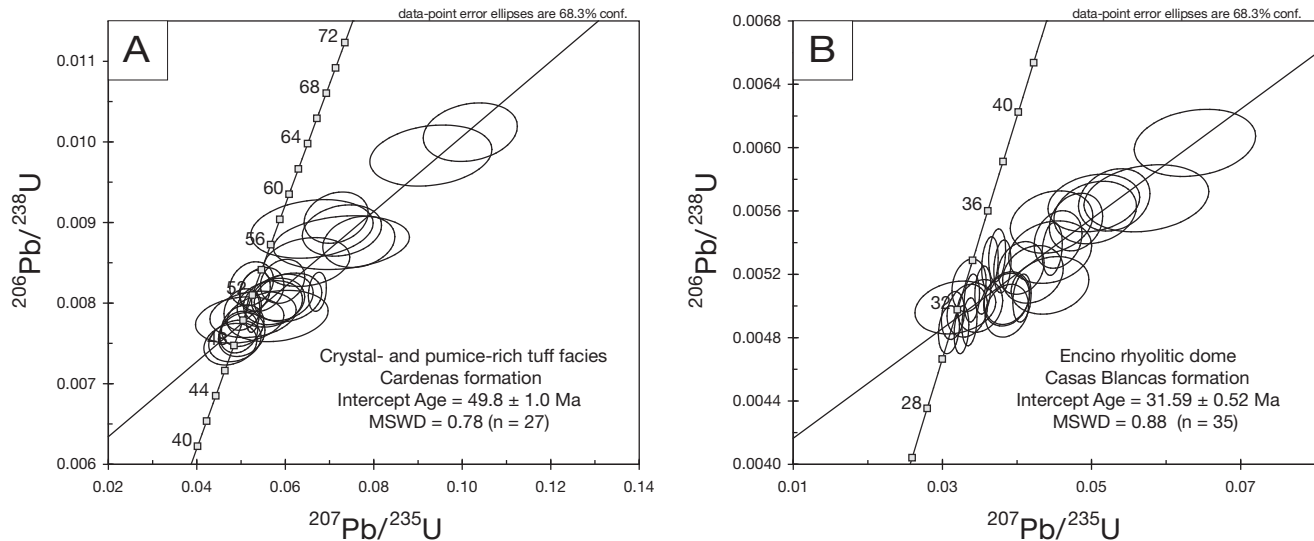


FIG. 6. $^{206}\text{Pb}/^{238}\text{Pb}$ vs. $^{207}\text{Pb}/^{235}\text{Pb}$ concordia diagrams for the crystal- and pumice-rich tuff facies of the Cardenas formation (A) and the Encino rhyolitic dome of the Casas Blancas formation (B). Error bars are 1 σ .

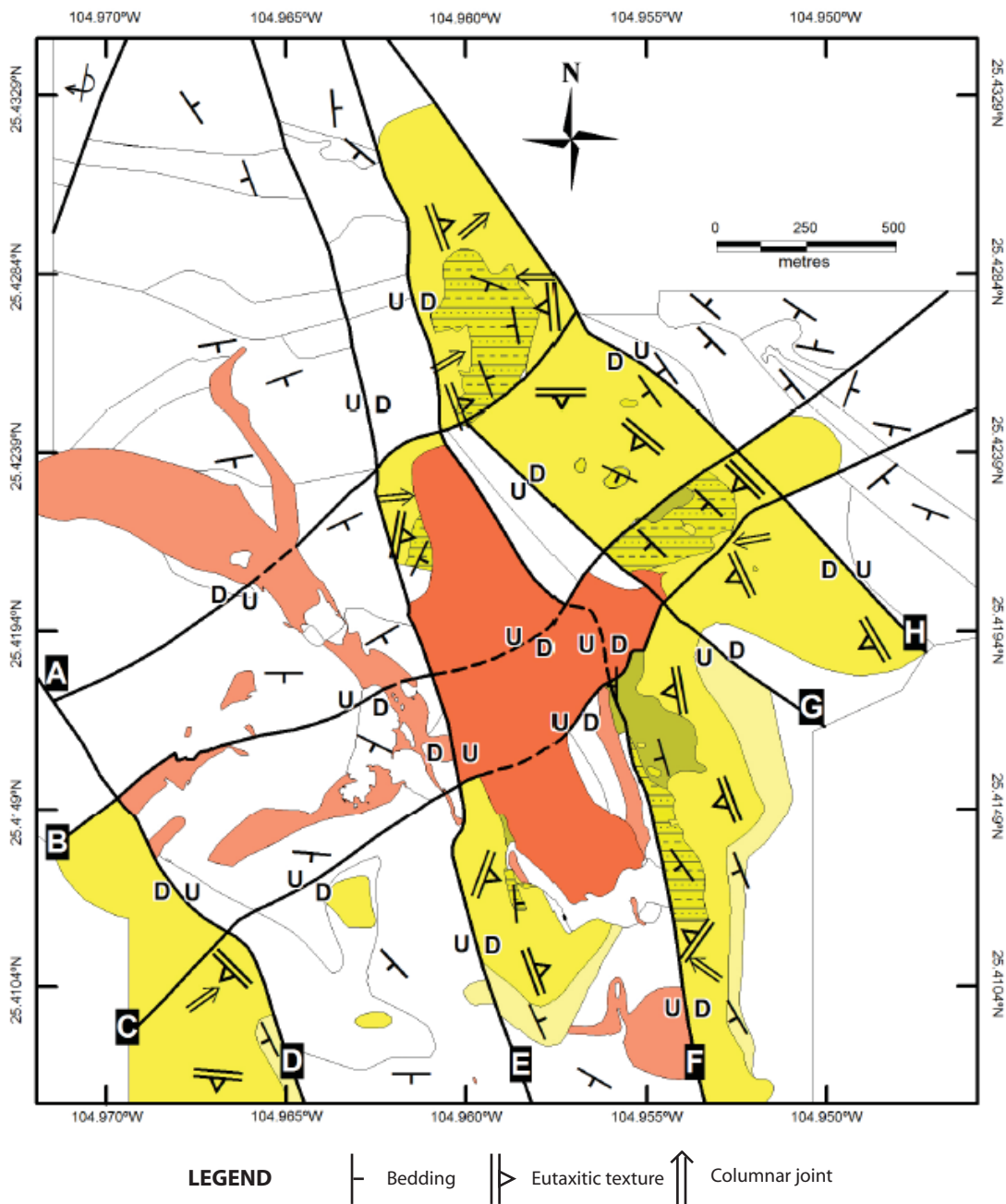


FIG. 7. Surface trace of faults that were active postemplacement of the Cardenas formation (legend as in Fig. 3). Vertical movements along the faults are indicated by "D" for down and "U" for up. Where the faults are represented by a dashed line, they are covered by the Encino rhyolitic dome lithofacies or crosscut by felsic intrusions.

felsic dikes and the two fault sets suggest that these faults, or ancillary parallel structures, were reactivated during volcanism that deposited the Casas Blancas formation and served as structural conduits for the felsic magma.

The protracted structural event is interpreted to correspond to an early Oligocene east-northeast-west-southwest extension that occurred along the eastern flank of the Sierra Madre Occidental volcanic province. This regional extensional event began about the same time as the Oligocene ignimbritic volcanism recorded in the Upper Volcanic Succession, and it faulted and tilted Eocene and early Oligocene

ignimbrites in the eastern flank of the central sector of the Sierra Madre Occidental (Aguirre-Díaz and McDowell, 1991, 1993; Luhr et al., 2001). This structural event was followed by a second erosional event that partially removed the Cardenas and Pitarrilla formations (Figs. 4, 5, 7), and it is marked by a well-defined angular unconformity between the Cardenas and Casas Blancas formations (Fig. 5).

Mineralization of the La Pitarrilla Deposit

Using descriptive criteria, mineralization at the La Pitarrilla deposit is subdivided into sulfide- and iron oxide-associated

styles (Figs. 8, 9). The laterally extensive iron oxide-associated and vertically extensive sulfide-associated mineralizations are collectively centered on Breccia Ridge, an area that is coincident with the intersection of rhyolitic dikes and sills defining the feeder system and vent area for the Encino rhyolitic dome (Figs. 8, 9).

Sulfide-associated mineralization

The sulfide-associated mineralization is most strongly developed below Breccia Ridge, in strata underlying the inferred

vent area for the Encino rhyolitic dome and within the core of the felsic dike complex (Figs. 8, 9). Here, the sulfide-associated mineralization extends from about 160 m below surface to vertical depths in excess of 930 m (using a 10 g/t Ag cutoff; Fig. 9). The sulfide-associated mineralization, having a maximum known lateral extent of 625 m in the northeast–south-southwest direction and about 1,000 m in the northeast-southwest direction, comes closest to surface along its western margin, and dips moderately to steeply eastward (Figs. 8, 9). The underground mineral resource of

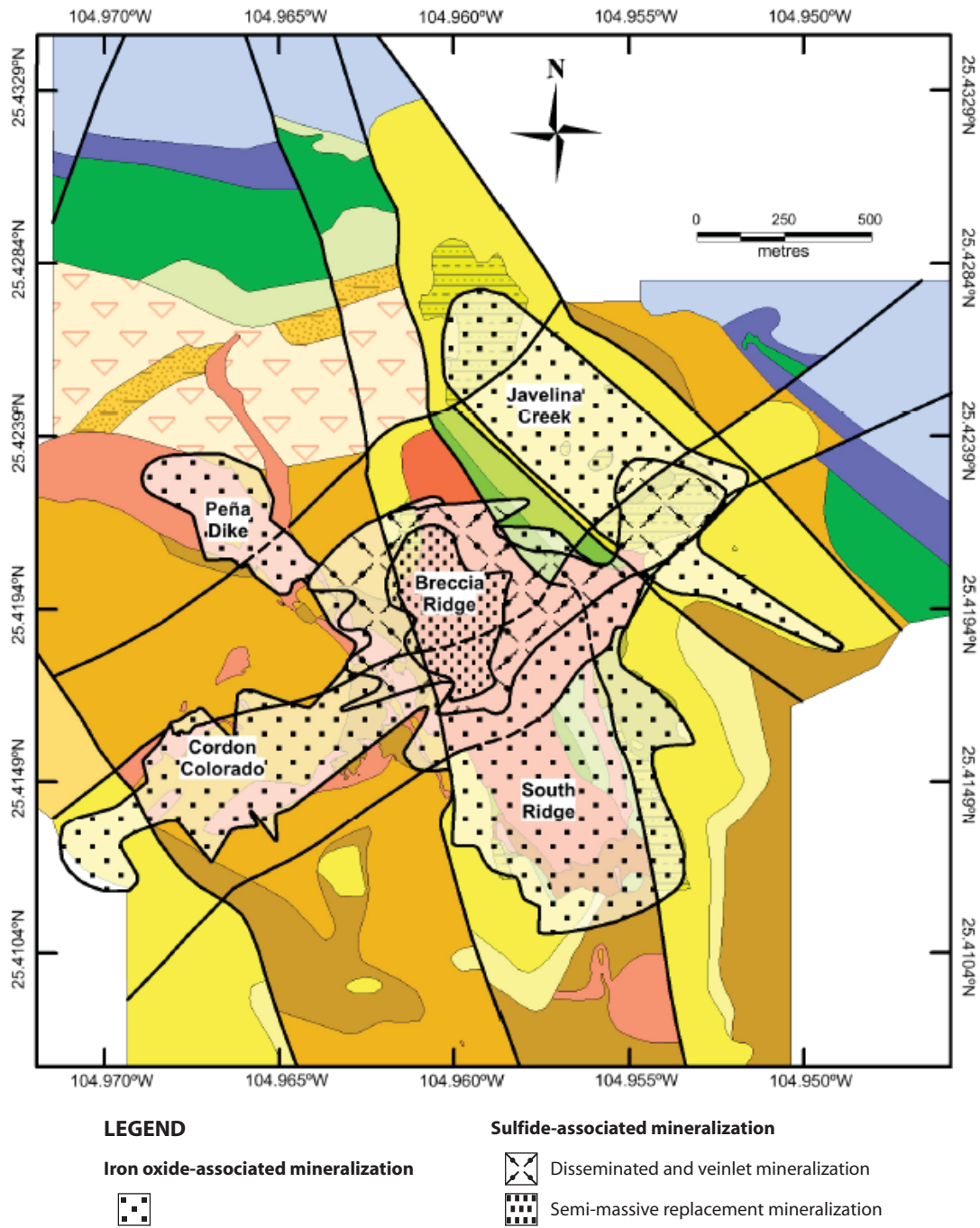


FIG. 8. Surface projection of the different styles of Ag-Zn-Pb mineralization (using a 10 g/t Ag cutoff) and the five mineralized zones recognized at the La Pitarilla deposit. Outcrops are removed for clarity (legend as in Fig. 3).

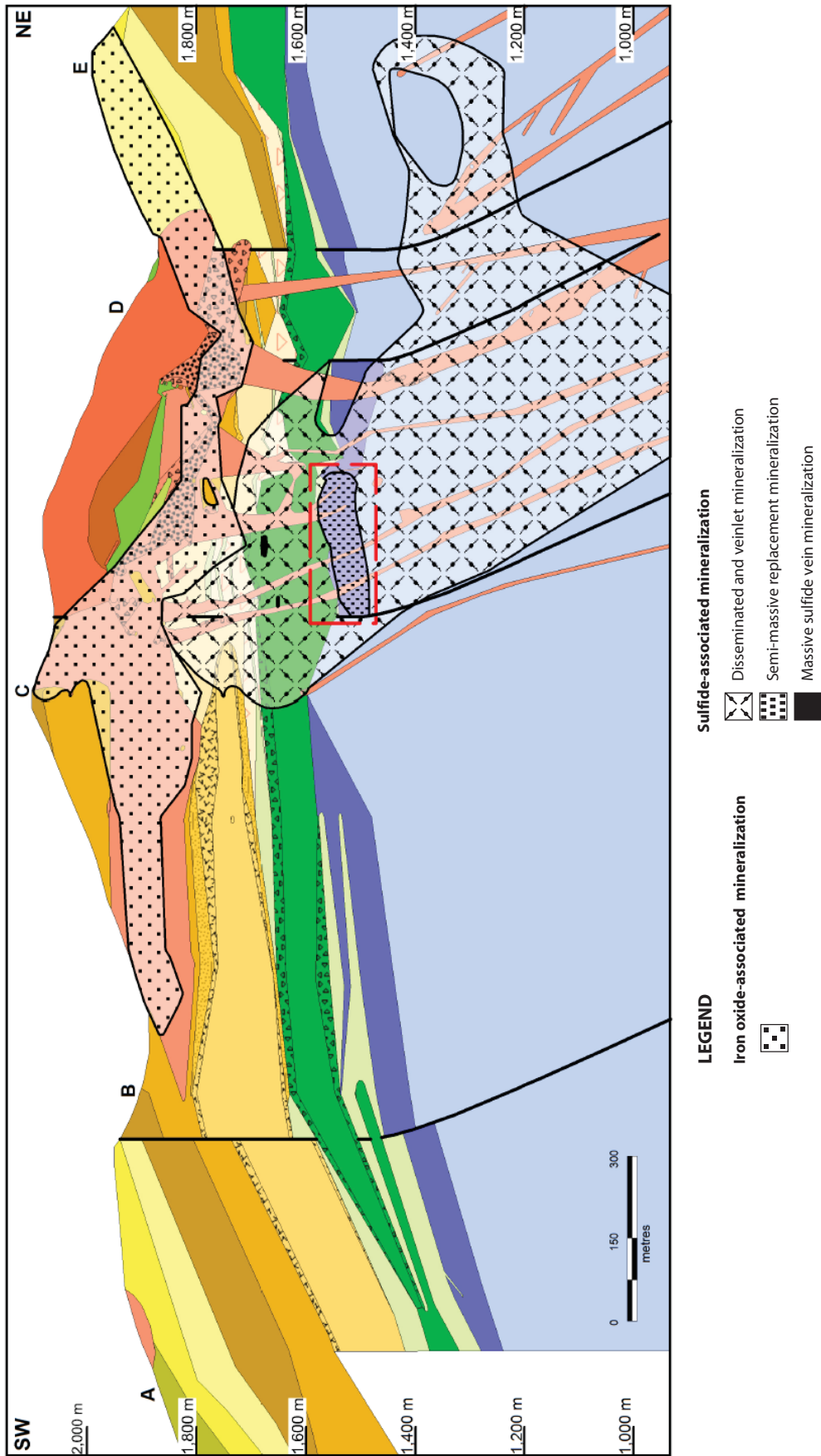


FIG. 9. Distribution of the different styles of Ag-Zn-Pb mineralization on the northeast-southwest section (10 g/t Ag grade was used to define the limits of the mineralization). The drill holes were removed for clarity. The red dashed rectangle highlights the location of semimassive replacement sulfide mineralization shown in Figure 11.

sulfide-associated mineralization at Breccia Ridge (measured and indicated categories) is estimated at 67 Mt based on a cutoff grade of 65 g/t Ag and is characterized by an average silver grade of 90 g/t Ag and a combined Zn + Pb content of about 2.2 percent (Wayne Ewert, 2008, pers. commun.).

Three different forms of sulfide-associated mineralization are recognized: (1) disseminated and veinlet mineralization (sphalerite, pyrite/marcasite, galena, chalcocopyrite, pyrrhotite, arsenopyrite \pm tetrahedrite, boulangerite, ullmannite, gersdorffite, and freislebenite); (2) semimassive replacement mineralization (sphalerite, pyrite/marcasite, pyrrhotite, chalcocopyrite, galena, arsenopyrite \pm tetrahedrite, stannite, and ramdohrite); and (3) massive sulfide vein mineralization (pyrite/marcasite, sphalerite, chalcocopyrite, galena, arsenopyrite, pyrrhotite \pm tetrahedrite, and miargyrite; Figs. 8–10).

Disseminated and veinlet mineralization represents the most voluminous form of sulfide-associated mineralization (Figs. 8, 9). It constitutes the stem of the mushroom-shaped La Pitarrilla deposit and is hosted by the Peña Ranch and Pitarrilla formations, the lower mafic sill, and the felsic dikes (Figs. 9, 10A, B). The <1- to 1-cm quartz \pm calcite-sulfide veins crosscut strata at variable angles, whereas the disseminated mineralization replaces the matrix and, to a lesser extent, clasts within beds and is best developed in proximity to the veinlets. The silver-bearing minerals are tetrahedrite, and less commonly, freislebenite. Typical alteration minerals associated with this mineralization include chlorite, iron carbonate, and kaolinite.

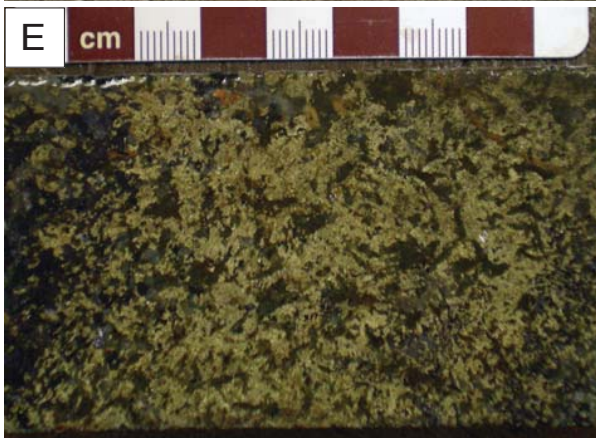
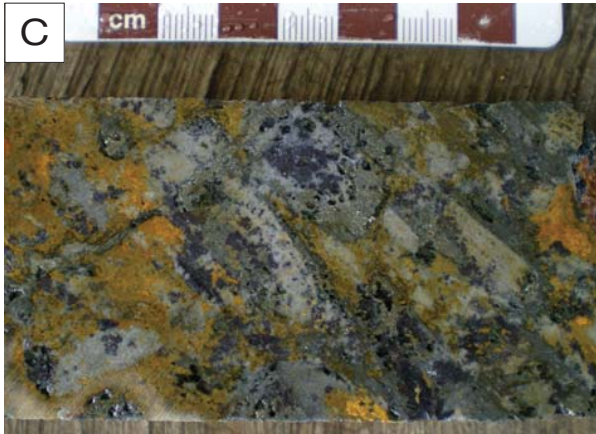
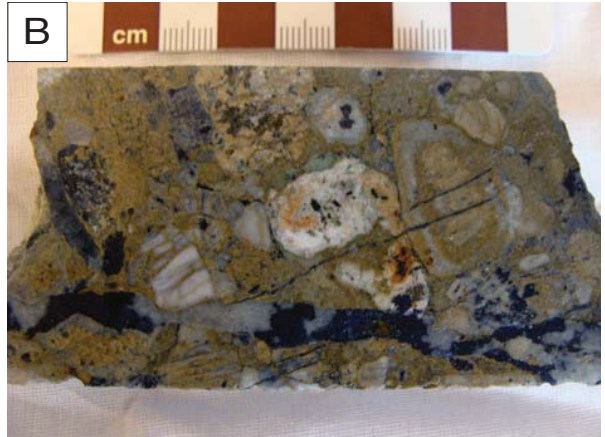
Semimassive replacement mineralization is restricted to conglomerates of the Manto Rico member where it occurs within an envelope of disseminated and veinlet mineralization (Fig. 9). It is the most important form of mineralization at La Pitarrilla as it contains an indicated mineral resource of 11 Mt with an average silver grade of 145 g/t Ag and a combined Zn + Pb content of about 4 percent (Anna Spieka, 2009, pers. commun.). The semimassive replacement mineralization is a strata-bound and flat-lying replacement-style mineralization in which sulfides and sulfosalts preferentially replaced limestone clasts along with other terrigenous sedimentary clasts and the matrix (Figs. 9, 10C, D). The semimassive replacement mineralization is divisible into four mineralogical zones (Fig. 11). These include the pyrrhotite, sphalerite, sphalerite-pyrite, and sphalerite-chalcocopyrite zones, in which each zone is dominated by one or two sulfide minerals and may contain up to 10 percent of other sulfides

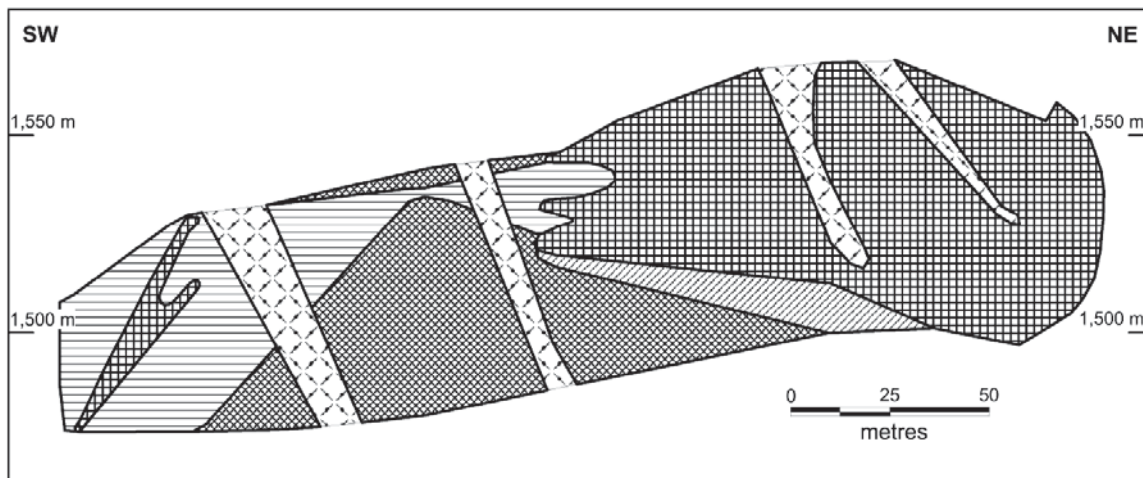
(Fig. 11). The distribution of mineralogical zones define a pronounced lateral and, to a lesser degree, vertical zoning where the sphalerite-chalcocopyrite zone defines the core of the replacement mineralization (Fig. 11). The sphalerite-pyrite and sphalerite-chalcocopyrite zones are economically most important as they contain the highest values in Ag, Zn, and Pb, especially where they are adjacent to felsic dikes. The silver-bearing minerals are tetrahedrite, and less commonly, ramdohrite. Alteration minerals include iron carbonate, chlorite, and sericite.

Massive sulfide vein mineralization is restricted to the lower mafic sill and, to a lesser extent, by felsic dikes (Fig. 9). It occurs above the semimassive replacement mineralization, i.e., within the upper part of the zone of disseminated and veinlet mineralization (Fig. 9). The massive sulfide veins occur as steeply dipping (40°–70°), decimeter- to meters-wide, mineralogically zoned, sharp-walled, and lesser breccia veins (Fig. 10E, F). The breccia veins contain jigsaw-fit to clast-rotated angular blocks of wall rock filled by comb quartz, and later sulfides (Fig. 10F). The sharp-walled veins occur separately or are superimposed on breccia veins and consist of massive sulfides with lesser quartz (often polyphase and colloform banded) and rare calcite (Fig. 10E). The massive sulfide veins can be subdivided into four styles based on mineralogy. These include marcasite-pyrite-sphalerite, chalcocopyrite-galena, arsenopyrite, and pyrrhotite-marcasite and/or pyrite veins. The most economically important veins are the chalcocopyrite-galena and arsenopyrite veins as they contain the highest values in Ag (Fig. 10E). The silver-bearing minerals are tetrahedrite, and less commonly, miargyrite. Alteration minerals for the massive sulfide vein mineralization are identical to the semimassive replacement mineralization.

The sulfide-associated mineralization consists mainly of disseminated and veinlet mineralization, which has been described in other Mexican epithermal deposits such as the Real de Ángeles deposit (Pearson et al., 1988). However, the semimassive replacement and massive sulfide vein mineralizations at La Pitarrilla are more common ore styles within the Mexican silver belt where the former is often referred to as manto style, and both styles occur together in some deposits such as at the Fresnillo (McDonald et al., 1986; Ruvalcaba-Ruiz and Thompson, 1988) and San Martín deposits (Rubin and Kyle, 1988). The sulfide-associated mineralization at La Pitarrilla, especially the disseminated and veinlet mineralization is interpreted to define the principal hydrothermal conduit for





FIG. 10. Mineralization styles at the La Pitarrilla deposit. A. Disseminated sphalerite interstitial to clasts within the heterolithic lithofacies of the Middle member, Pitarrilla formation (231 g/t Ag, 11,700 ppm Zn, and 3,380 ppm Pb). Note the disseminated iron carbonate alteration of the clasts. B. Irregular quartz vein containing sphalerite cutting conglomerate of the Peña Ranch formation that also contains disseminated sphalerite within the matrix and in some clasts (102 g/t Ag, 33,000 ppm Zn, and 11,900 ppm Pb). Clasts and matrix show iron carbonate alteration. C. Replacement of the Manto Rico member conglomerate by pyrrhotite. The clastic texture of the conglomerate is not apparent due to strong iron carbonate and patchy chlorite alteration (40.6 g/t Ag, 12,000 ppm Zn, and 3,570 ppm Pb). D. Sphalerite and pyrite partially and preferentially replacing tabular carbonate clasts of the Manto Rico member (114 g/t Ag, 20,400 ppm Zn, and 9,210 ppm Pb). The matrix shows strong iron carbonate alteration. E. Massive sulfide vein cutting the lower mafic sill that contains chalcocopyrite and marcasite with disseminated sphalerite (1,200 g/t Ag, 39,000 ppm Cu, 67,000 ppm Zn, and 4,000 ppm Pb). F. Breccia vein that contains jigsaw-fit angular blocks of the lower mafic sill filled by comb quartz, and later sulfides (230 g/t Ag, 100,500 ppm Zn, and 4,030 ppm Pb). G. Iron oxide-associated silver mineralization hosted by a hematite-altered felsic sill at Cordon Colorado (6.9% Fe; 31.5 g/t Ag, 826 ppm Zn, and 1,270 ppm Pb; orange X = 1 cm). H. Iron oxide-associated silver mineralization hosted by a hematite-altered felsic sill at Cordon Colorado (8.9% Fe; 1,600 g/t Ag, 1,410 ppm Zn, and 10,600 ppm Pb; orange X = 1 cm).





LEGEND

Mineralogical zones of the semi-massive replacement mineralization

-  Pyrrhotite
-  Sphalerite
-  Sphalerite-pyrite
-  Sphalerite-chalcopyrite

Disseminated and veinlet mineralization



FIG. 11. Distribution of the sulfide replacement zones within the semimassive replacement sulfide mineralization on the northwest-southeast cross section (see Fig. 9 for the location of the semimassive replacement sulfide mineralization).

ascending hydrothermal fluids where the silver and base metals precipitated.

Iron oxide-associated mineralization

The iron oxide-associated mineralization represents the cap of the mushroom-shaped La Pitarrilla deposit. It is the most laterally extensive mineralization style and forms five partially connected zones referred to as Cordon Colorado, Peña Dike, Javelina Ridge, South Ridge, and Breccia Ridge (Figs. 8, 9). According to publicly released company resource estimates (James McCrea, 2006, pers. commun.; Wayne Ewert, 2008, pers. commun.), the five zones of iron oxide-associated mineralization contain a total of approximately 169 Mt of mineral resources in the measured and indicated categories, using a 20 g/t Ag cutoff grade for the Breccia Ridge zone and a 40 g/t Ag cutoff grade for the other zones. The silver grades for the five near-surface zones average between 80 and 125 g/t Ag. The areal extent of the mineralization as a whole is considerable, about 1.9 km in the north-northwest–south-southeast direction and 2.3 km in the northeast-southwest direction (Fig. 8). This style of mineralization is typically found within 100 m of surface; however, at Breccia Ridge it is encountered at depths up to 450 m (Fig. 9).

Rhyolitic sills and dikes and the base of the Encino rhyolitic dome are the main host rocks for the mineralization in the Cordon Colorado, Peña Dike, South Ridge, and Breccia Ridge zones, while at Javelina Ridge and South Ridge the crystal-rich pumice tuff and stratified tuff lithofacies of the Cardenas formation are the principal host rocks (Figs. 8, 9).

Geochemically anomalous concentrations of Zn (>2,000 ppm) and Pb (>500 ppm) are commonly associated with the iron oxide-associated mineralization with the highest concentrations of these metals occurring in rocks directly above the sulfide-associated mineralization that constitutes the bulk of the Breccia Ridge zone.

The iron oxide-associated mineralization is characterized by disseminated and fracture-controlled hematite, limonite, and lesser manganese and titanium oxides, the latter including cesarolite, coronadite, hollandite, and rutile (Peter Le Couteur, 2006, pers. commun.; Fig. 10G, H). The most strongly hematite altered samples are characterized by the highest values of Fe but are not necessarily associated with the highest values in Ag, Zn, and Pb. This indicates that iron staining or degree of oxidation is not a viable criterion for identifying higher Ag or base metal grades (Fig. 10G, H).

The iron oxide-associated mineralization is composed of base metal sulfide and silver minerals that are visible only at the micron scale, except for pyrite. The base metal sulfides include pyrite, sphalerite, galena, chalcopyrite, as well as minor cinnabar and covellite (Peter Le Couteur, 2006, pers. commun.). The silver minerals occur as micron-sized grains (<30 μm large) and include abundant acanthite and lesser silver halides (iodargyrite, chlorargyrite, and bromargyrite) with rare silver selenides and sulfo-selenides (naumannite and agularite) and silver-mercury-iodide-sulfides (probable imiterite and Hg iodargyrite; Peter Le Couteur, 2006, pers. commun.). The silver grains are scattered throughout the host rock and do not show any preferential spatial relationship

with the phenocrysts of the host rock (quartz, feldspar, and K-feldspar) or the intensity of oxide alteration (Peter Le Couteur, 2006, pers. commun.). The dominant alteration minerals associated with the iron oxide-associated mineralization are nontronite, halloysite, montmorillonite, illite, tourmaline, kaolinite, buddingtonite, muscovite, alunite, and anhydrite.

The iron oxide-associated mineralization is similar to oxide mineralization described in some epithermal precious and base metal deposits elsewhere in the Mexican silver belt where it is intimately associated with sulfide-silver epithermal veins and typically overprints sulfide mineralization (Lyons, 1988; Moller et al., 2001; Zawada et al., 2001). However, the strong lithologic control on the iron oxide-associated mineralization, which is mainly hosted by the felsic intrusions and the rhyolitic dome, is either unique to La Pitarrilla or has not been documented in other Mexican deposits. Although sparsely documented, oxide mineralization in the Mexican silver belt is interpreted to have formed during supergene weathering of the early hypogene sulfide mineralization (Gemmell et al., 1988; Zawada et al., 2001).

At Pitarrilla, the downward gradation of iron oxide-associated mineralization into the sulfide-associated mineralization and the common base metal content and sulfide minerals for both mineralization styles suggest that the iron oxide-associated mineralization resulted from the supergene oxidation of hypogene sulfide-associated mineralization. In this scenario, silver would have been liberated from the original silver-bearing minerals within the sulfide-associated mineralization during oxidation and moved into new silver minerals that are stable in the near-surface environment, i.e., acanthite, and lesser silver halides with rare silver selenides and sulfo-selenides, and silver-mercury-iodide-sulfide. The disseminated and fracture-controlled hematite and limonite would be products of oxidation of the associated hypogene sulfides. The common association of the oxide-associated mineralization with felsic intrusions suggests that the distribution and concentration of the original hypogene sulfide-associated mineralization was, in part, lithologically controlled. The timing of the mineralization is uncertain, but given that the base of the Encino rhyolitic dome is weakly mineralized by the iron oxide-associated mineralization, it is interpreted to have occurred during or after emplacement of the Encino rhyolitic dome.

Tourmaline alteration

Jigsaw-fit to clast-rotated breccias that contain angular clasts of their coherent and volcanoclastic host rocks occur throughout the La Pitarrilla deposit area but are best developed within strata adjacent to and within the felsic dike complex that defines the vent area for the Encino rhyolitic dome at Breccia Ridge (Figs. 4, 5). The matrix of the breccias locally consists of a fine-grained, black intergrowth of quartz, tourmaline, potassium feldspar, and lesser pyrite, which appear to replace a rock flour matrix or, in some examples, may represent an open-space infilling. Although sphalerite, pyrite, and minor to trace amounts of galena, and Pb-Sb (-Ag) sulfosalts occur locally in the breccias, they are not a common host rock for mineralization at La Pitarrilla and their relationship, besides spatial, to the silver and base metal mineralization as well as their origin is presently uncertain.

The jigsaw-fit breccias possess features that are similar to diatreme breccias described in association with magmatic-hydrothermal ore deposits in volcano-plutonic arcs (Sillitoe and Bonham, 1984; Sillitoe, 1985, 1997; Lorenz, 1986); however, as the breccias cannot be unequivocally linked to maar volcanism at La Pitarrilla, they are referred to as diatreme-like breccias. Although the tourmaline (quartz) mineralized diatreme-like breccias are spatially associated with the silver and base metal mineralization, tourmaline is not a typical mineral associated with epithermal deposits, except for some epithermal deposits such as the Sari Gunay epithermal gold deposit in Northwest Iran in which the tourmaline alteration is hosted by hydrothermal breccias (Richards et al., 2006). However, tourmaline is a common mineral within magmatic breccias associated with porphyry deposits (Sillitoe, 2010).

Discussion and Conclusions

The present study shows that the sedimentary environment prevailing during deposition of the middle Cretaceous Peña Ranch formation did not influence mineralization at La Pitarrilla. The Peña Ranch formation is the stratigraphic equivalent of the regional Mezcalera Formation and forms the basement to Eocene and Oligocene volcanic edifices, which unconformably overlie this formation. The Cretaceous-Eocene unconformity is regional in extent and is marked by heterolithic conglomerates, which at La Pitarrilla are represented by the Manto Rico member (Figs. 2–5).

In contrast to the Peña Ranch formation, investigation of the Eocene to Oligocene strata unraveled the geologic history of the La Pitarrilla Ag-Zn-Pb deposit, which is summarized in chronological order below, with the last event being the formation of the mineralization (Fig. 12).

Volcanoclastic lithofacies of the Eocene Pitarrilla formation are interpreted to have been derived from arc volcanoes (Fig. 12A); even the conglomerate lithofacies of the Manto Rico member contains volcanic clasts of arc derivation. This is consistent with the mineralogy (feldspar, amphibole, pyroxene, and biotite porphyritic; App.) and the composition (negative Nb, Ta, Ti anomalies, and steep REE pattern on primitive mantle normalized plots; App.) of clasts within the volcanoclastic strata. The heterolithic character of clasts within most of the volcanoclastic deposits along with the rounding of the clasts suggest their derivation from primarily unconsolidated arc pyroclastic deposits, their redeposited equivalents and, to a lesser extent, through the weathering and erosion of consolidated deposits. Monolithic volcanoclastic deposits that are intercalated with heterolithic volcanoclastic deposits are interpreted to be primary pyroclastic deposits derived from submarine or subaerial arc eruptions. The latter interpretation implies proximity to the former arc, as does the occurrence of a thick, coherent andesitic flow that indicates the La Pitarrilla depositional basin was also a localized eruptive center during the Eocene (Fig. 12B).

Cohesive debris flows and low- and high-density turbidity currents were the primary transport mechanisms for the volcanoclastic arc debris and primary pyroclastic ejecta. Based on the tuff to tuff breccia clast size range of the particulate gravity flow deposits, the Pitarrilla formation strata are interpreted to be part of a gravel-rich marine clastic system (Richards and Bowman, 1998). The wide range of volcanic

clast compositions suggests multiple volcanic sources, which is consistent with a linear arc source that allowed the construction of a gravel-rich slope-apron system off the flank of the former arc and into a back-arc extensional basin (Richards and Bowman, 1998; Richards et al., 1998). Here the volcanoclastic deposits accumulated below storm wave base and within marine basins. Pitarrilla formation strata are interpreted to represent the erosional remnants of one such basin that was likely fault controlled and whose margins, in part, may have exposed the older Cretaceous sedimentary strata (Fig. 12A). The occurrence of siltstone and mudstone clasts within heterolithic volcanoclastic deposits is consistent with their derivation from identical lithofacies within the underlying Cretaceous sedimentary strata either during transport of debris from the arc or directly from the margins of a fault-controlled depositional basin (Fig. 12A).

Eocene uplift, which has not been previously documented within the eastern flank of the central sector of the Sierra Madre Occidental, is interpreted to have uplifted Eocene volcanoclastic strata at La Pitarrilla to a subaerial environment and to have resulted in the Plinian eruptions that formed the ignimbrite deposits of the Lower Volcanic Succession. At La Pitarrilla, pyroclastic deposits correlative with the silicic volcanism of Lower Volcanic Succession are represented by the subaerial, crystal-rich, welded and nonwelded ignimbrites and pyroclastic surge deposits of the Cardenas formation (49.8 ± 1.0 Ma; Fig. 12C, D). Following the eruption and emplacement of the Lower Volcanic Succession ignimbrites, the La Pitarrilla area experienced extensive erosion of the ignimbrite and pyroclastic surge deposits, and a return to a marine or lacustrine environment under which the stratified lithofacies of the Cardenas formation were deposited. It is unknown if this marine or lacustrine setting was regionally extensive along the eastern flank of the central sector of the Sierra Madre Occidental or if it was localized to specific areas such as at La Pitarrilla.

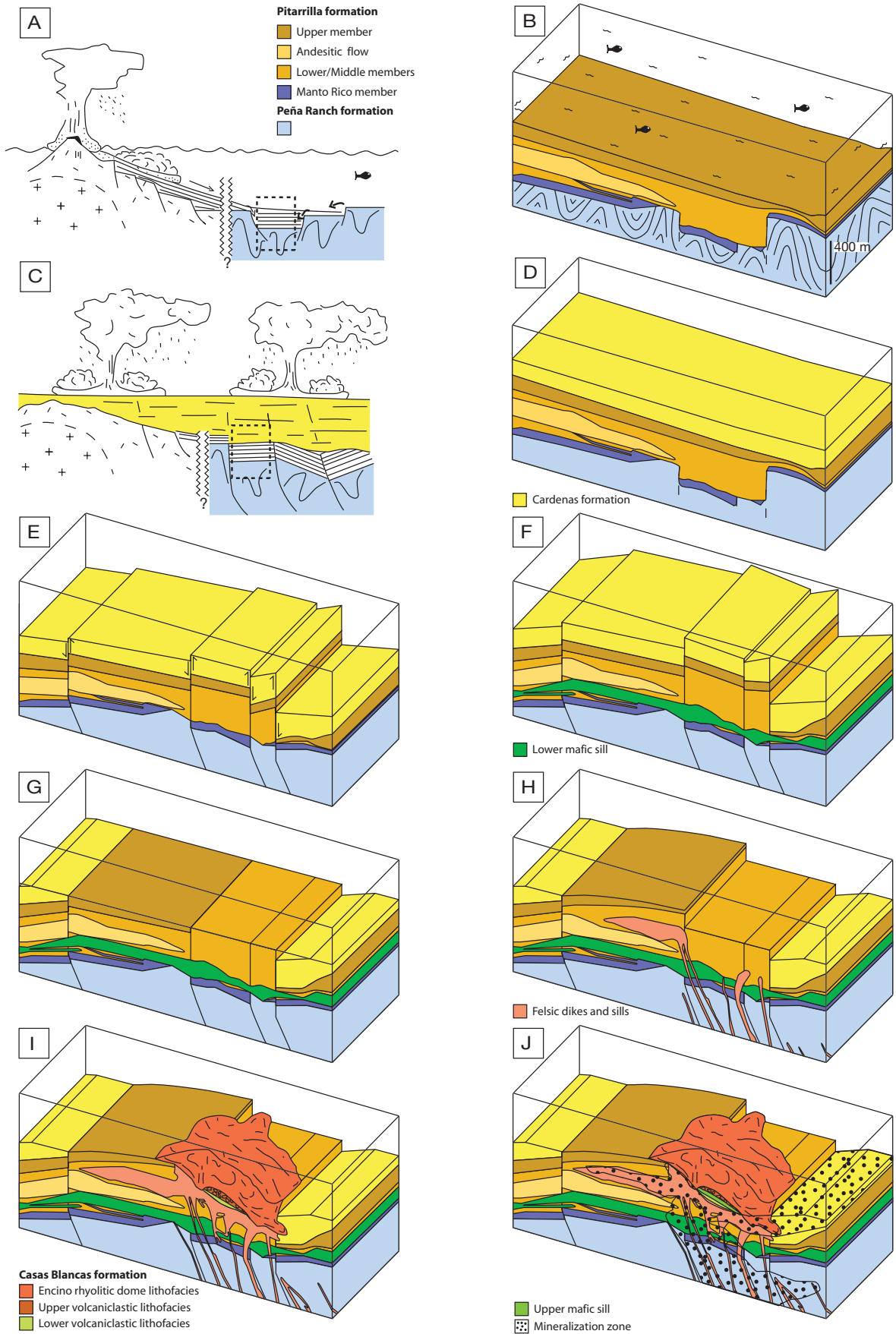
An early Oligocene east-northeast–west-southwest extensional event manifest by the northeast- and north-northwest–trending, steeply dipping listric faults resulted in tilting of the Pitarrilla and Cardenas formations and erosion of the Cardenas formation ignimbrite and pyroclastic surge deposits, the underlying Pitarrilla formation volcanoclastic rocks (Fig. 7) along with the development of an angular unconfor-

mity between the Cardenas and Casas Blancas formations (Fig. 12E, G).

Emplacement of the lower mafic sill into unconsolidated volcanoclastic rocks of the La Pitarrilla formation may have occurred during erosion of the Cardenas formation but followed cessation of significant early Oligocene extension and faulting at La Pitarrilla as the northeast- and north-northwest–trending faults do not measurably displace the lower mafic sill (Fig. 12F). The calc-alkaline, andesitic lower mafic sill has arc-like affinities (App.).

Renewed silicic volcanism, initially marked by the emplacement of rhyolitic sills and dikes, immediately followed the emplacement of the lower mafic sill. This is interpreted to have been accompanied by doming at La Pitarrilla and reactivation of the northeast- and north-northwest–trending faults due to the emplacement of felsic intrusions along these planes of weakness, which induced the development of localized basins at surface (Fig. 12H). The areally restricted, relatively flat-lying, lower volcanoclastic lithofacies of the Casas Blancas formation was deposited within the shallow marine or lacustrine basin that occupied the La Pitarrilla area during the Oligocene (Fig. 12H, I). Silicic volcanism continued with the Encino rhyolitic dome (31.59 ± 0.52 Ma) that was emplaced within fault-controlled topographic depressions or sub-basins that presumably developed as local extension continued and normal faulting progressed (Fig. 12I). Some of the felsic dikes undoubtedly represent the feeders to the dome. Mass wasting or mild volcanic explosions are believed to have occurred during initial emplacement of the Encino dome and contributed rhyolitic detritus to contemporaneously deposited volcanoclastic deposits of the upper volcanoclastic lithofacies of the Casas Blancas formation, which eventually were buried by the advancing dome. It is uncertain if the hyaloclastite at the base of the dome formed through the interaction with water-saturated volcanoclastic material during emplacement in a localized marine or lacustrine environment. As the top of the Encino rhyolitic dome is not preserved, it is uncertain if the dome was emplaced in an entirely subaqueous environment or if it was emergent. The occurrence of peperite within the upper mafic sill supports both interpretations. The nearly contemporaneous timing of upper mafic sill and Encino rhyolitic dome emplacement suggest that La Pitarrilla is a bimodal volcanic center (Fig. 12J).

FIG. 12. Diagram depicting the evolution of volcano-sedimentary environments at La Pitarrilla. A. Volcanoclastic deposits derived through arc volcanism and erosion of subaerial volcanoes, transport by particulate gravity flows, and deposition within a back-arc extensional setting (dashed square denotes the La Pitarrilla deposit area). B. The La Pitarrilla basin with deposition of volcanoclastic rocks in a below storm wave base marine environment. The andesitic flow indicates arc-like volcanism within the depositional basin. C. Eocene arc uplift, erosion, and extension associated with voluminous silicic pyroclastic volcanism that formed the voluminous ignimbrite deposits of the Lower Volcanic Succession (dashed square denotes the La Pitarrilla deposit area). D. At La Pitarrilla, the voluminous silicic volcanism is manifested by nonwelded to welded ignimbrite and pyroclastic surge deposits of the Cardenas formation. E. At the scale of the La Pitarrilla deposit, northeast- and north-northwest–trending steeply dipping listric faults caused faulting and tilting of the Pitarrilla and Cardenas formations. Faulting corresponds to regional early Oligocene east-northeast–west-southwest extension of the eastern flank of the Sierra Madre Occidental volcanic province. F. Emplacement of the lower mafic sill. G. Eocene to early Oligocene erosion of the faulted and tilted Pitarrilla and Cardenas formations. H. Initial emplacement of felsic intrusions that resulted in uplift and doming of the overlying strata. I. Emplacement of the Casas Blancas formation, which consists of two flat-lying volcanoclastic deposits overlain by a Encino rhyolitic dome complex that belongs to the Oligocene Upper Volcanic Succession that was emplaced, in whole or in part, in a subaqueous environment. J. Emplacement of the upper mafic sill and the mineralization during or just after emplacement and growth of the Encino rhyolitic dome complex.



The sulfide- and iron oxide-associated silver and base metal mineralization at La Pitarrilla are interpreted to be part of a single, vertically stacked, mineralized deposit where the styles of mineralization change with depth and, to a lesser extent, with host-rock type and by supergene weathering processes (Figs. 8, 9). Sulfide-associated mineralization occurs at depth and forms an areally restricted but vertically extensive zone that is rooted in the Cretaceous basement, and extends into the overlying Eocene volcanoclastic strata (Fig. 9). Throughout most of its vertical extent, the sulfide-associated mineralization occurs as disseminated, fine-grained, sulfide aggregates, and veinlets. Strata-bound, semimassive replacement mineralization, which is found almost exclusively within the Manto Rico member, is an example of where a compositionally receptive lithology, in this case abundant limestone clasts and, perhaps, a more permeable rock type, in this case framework-supported granule to cobble conglomerates, resulted in replacement-style mineralization prevailing over the disseminated and vein style of mineralization. The decimeter- to meters-wide, mineralogically zoned colloform banded quartz-sulfide veins, typical of many other Mexican silver vein deposits (e.g., Camprubí and Albinson, 2007), are best developed within lower mafic sill. The preferential development of mineralogically zoned veins within the lower mafic sill may reflect the lower permeability and more competent nature of this sill where, and, as proposed by Sillitoe (1993) for epithermal deposits, fluid overpressure below this coherent intrusion may have resulted in brittle failure of the lower mafic sill and the development of breccia and sharp-walled veins. The mainly discordant, sulfide-associated mineralized zone continues upward through Eocene and Oligocene volcanoclastic rocks where it abruptly changes into a laterally extensive, but vertically limited zone of disseminated and, to a lesser extent, fracture-controlled sulfide-silver mineralization that was subsequently oxidized during supergene weathering (Fig. 9). The horizontally extensive nature of this originally disseminated sulfide zone is interpreted to reflect an abrupt change in horizontal permeability afforded by the host strata, primarily felsic sills and, to a lesser extent, unconsolidated Eocene and Oligocene volcanoclastic strata.

The timing of the mineralization is uncertain, but given that the base of the Encino rhyolitic dome is weakly mineralized by the iron oxide-associated mineralization, it is interpreted to have occurred during or after emplacement of the Encino rhyolitic dome (<31.6 Ma). This suggests that the Ag-Zn-Pb mineralization event occurred within a subaqueous or emergent environment or within an emergent to subaerial environment after Encino rhyolitic volcanism (Fig. 12J); a subaqueous or emergent environment is not typical environment in models for epithermal precious metal deposits. The volcanic structural control on the mineralization is evident. Northeast- and north-northwest-trending faults that developed during the early Oligocene were reactivated just after the extension as they not only controlled the location of the Encino rhyolitic dome but also the Ag-Pb-Zn mineralization.

Features of the La Pitarrilla deposit that are typical of epithermal precious and base metal deposits within the Mexican silver belt include vein, manto, and oxide mineralization styles, silver and base metal signatures (base metal sulfides and Ag, Pb, Cu, Sb sulfosalts), and postsubduction extensional

tectonism. Camprubí and Albinson (2007) proposed a new classification scheme for Mexican epithermal deposits (A, B, and C) where type A deposits are defined exclusively by polymetallic intermediate-sulfidation mineralization. Type B deposits are those that exhibit predominantly low-sulfidation mineralization but have polymetallic intermediate-sulfidation roots (Zn-Pb-Cu). Type C deposits possess classic low-sulfidation mineralization. The sulfide mineralogy at the La Pitarrilla deposit suggests that it is a type A deposit, although the association of mineralization with extension and felsic domes is characteristic of type B deposits.

Exploration Implications

The study of the La Pitarrilla Ag-Zn-Pb deposit highlighted the role of structural controls on volcanism and deposit formation. Early synvolcanic faults that controlled basin development and volcanoclastic sedimentation during Eocene volcanism (andesitic flow) and extension were reactivated during the Oligocene. At this time, these structures controlled the location of the bimodal rhyolitic and andesitic volcanism and the Ag-Zn-Pb mineralization. These observations and the volcanic reconstruction at La Pitarrilla suggest that reactivation of older synvolcanic and extensional structures may be key to the location of Mexican epithermal precious metal deposits.

Oligocene bimodal volcanic centers (Oligocene rhyolitic domes and intrusions, and andesitic intrusions) may define potentially favorable environments for epithermal precious metal deposits in Mexico.

The La Pitarrilla Ag-Zn-Pb deposit may represent a completely preserved vertically stacked mineralized system in which disseminated, replacement, vein, and supergene-altered disseminated and fracture-controlled sulfide mineralization occur within a single deposit. Thus, areas or prospects that contain one or more of the mineralization styles, even if subeconomic, may have the potential to host other economic mineralization styles. This is particularly true for prospects with oxidized mineralization that may have been overlooked in exploration programs and have the potential to overly more deeply seated vein- and/or replacement-style deposits.

The less recognized, iron oxide-associated mineralization has the potential to add significant tonnage and, therefore, to contribute to the economic potential of Mexican epithermal precious and base metals deposits. The potential of this mineralization is further enhanced by its accessibility from surface operations.

At La Pitarrilla, the silver- and base metal-rich replacement mineralization preferentially developed within limestone clast-bearing conglomerates that occur at the Cretaceous-Eocene unconformity. The regional extent of the Cretaceous-Eocene unconformity and the limestone clast-bearing conglomerates represent a potential target interval especially in mineralized districts where silver and base metal mineralization has been discovered above the unconformity.

Acknowledgments

We thank Silver Standard Resources Inc. for initiating this research project and for their financial and logistical support. Financial support was also provided by a Natural Science and Engineering Research Council of Canada Discovery Grant to HLG. In particular, we thank Francisco Loera, Paul Bowen,

and Martin Samilpa-Viramontes for the assistance they provided during the senior author's fieldwork and for guidance at various stages of the project. We are also grateful to Eduardo Antonio Villa de la Torre for his assistance in the field, Humberto Martos del Rivero for digitizing the geologic map, and Bruno Lafrance, Balz Kamber, Pedro Jugo, and Darrel Long for helpful discussions on the geology of La Pitarrilla. Insightful reviews by Gerardo J. Aguirre-Díaz and Stuart F. Simmons are acknowledged. Richard J. Goldfarb, Erin Marsh, and Thomas Monecke are thanked for their incisive and constructive criticisms and insights that considerably improved earlier versions of the manuscript.

REFERENCES

- Aguirre-Díaz, G.J., and Labarthe-Hernández, G., 2003, Fissure ignimbrites: Fissure-source origin for voluminous ignimbrites of the Sierra Madre Occidental and its relationship with Basin and Range faulting: *Geology*, v. 31, p. 773–776.
- Aguirre-Díaz, G.J., and McDowell, F.W., 1991, The volcanic section at Nazas, Durango, Mexico, and the possibility of widespread Eocene volcanism within the Sierra Madre Occidental: *Journal of Geophysical Research*, v. 96, p. 13373–13388.
- 1993, Nature and timing of faulting and syn-extensional magmatism in the southern Basin and Range, central-eastern Durango, Mexico: *Geology Society of America Bulletin*, v. 105, p. 1435–1444.
- Aguirre-Díaz, G.J., Labarthe-Hernández, G., Tristán-González, M., Nieto-Obregón, J., and Gutiérrez-Palomares, I., 2008, The ignimbrite flare-up and graben-calderas of the Sierra Madre Occidental, Mexico: *Developments in Volcanology*, v. 10, p. 143–180.
- Allen, S.R., Hayward, B.W., and Mathews, E., 2007, A facies model for a submarine volcanoclastic apron: The Miocene Manukau Subgroup, New Zealand: *Geological Society of America Bulletin*, v. 119, p. 725–742.
- Andersen, T., 2002, Correction of common lead in U-Pb analyses that do not report ^{204}Pb : *Chemical Geology*, v. 192, p. 59–79.
- Aranda-Gómez, J.J., and McDowell, F.W., 1998, Paleogene extension in the southern Basin and Range province, Mexico: Syndepositional tilting of Eocene red beds and Oligocene volcanic rocks in the Guanajuato mining district: *International Geology Review*, v. 40, p. 116–134.
- Araujo-Mendieta, J., and Arenas-Partida, R., 1986, Estudio tectónico-sedimentario en el Mar Mexicano, estados de Chihuahua y Durango: *Sociedad Geológica Mexicana Boletín*, v. 47, p. 43–88.
- Batiza, R., and White, J.D.L., 2000, Submarine lavas and hyaloclastite in Sigurdsson, H., ed., *Encyclopedia of volcanoes*: London, Academic Press, p. 361–382.
- Benn, K., and Kamber, B.S., 2009, In situ U/Pb granulite-hosted zircon dates, Kapuskasing structural zone, Ontario: A late Archean Large Igneous Province (LIP) as a substrate for juvenile crust: *Journal of Geology*, v. 117, p. 519–541.
- Bralower, T.J., Fullagar, P.D., Paull, C.K., Dwyer, G.S., and Leckie, R.M., 1997, Mid-Cretaceous strontium-isotope stratigraphy of deep-sea sections: *Geological Society of America Bulletin*, v. 109, p. 1421–1442.
- Branney, M.J., and Kokelaar, P., 2002, Pyroclastic density currents and the sedimentation of ignimbrites: *Geological Society of London Memoir* 27, 143 p.
- Camprubí, A., and Albinson, T., 2007, Epithermal deposits in Mexico—update of current knowledge, and an empirical reclassification: *Geology Society of America Special Paper* 422, p. 377–415.
- Camprubí, A., Ferrari, L., Cosca, M.A., Cardellach E., and Canals, À., 2003, Ages of epithermal deposits in Mexico: Regional significance and links with the evolution of Tertiary volcanism: *ECONOMIC GEOLOGY*, v. 98, p. 1029–1037.
- Cas, R.A.F., and Wright, J.V., 1987, Volcanic successions: Modern and ancient. A geological approach to processes, products and successions: London, Allen and Unwin, 528 p.
- Damon, P.E., Shafiqullah, M., and Clark, K.F., 1981, Age trends of igneous activity in relation to metallogenesis in the southern Cordillera: *Arizona Geological Society Digest*, v. 14, p. 137–153.
- De La Garza, V., Olavide, S., and Villasuso, R., 2001, Geology and ore deposits of the La Ciénega gold district, Durango, México: *Society of Economic Geologists Special Publication* 8, p. 87–93.
- Dickinson, W.R., and Lawton, T.F., 2001, Carboniferous to Cretaceous assembly and fragmentation of Mexico: *Geology Society of America Bulletin*, v. 113, p. 1142–1160.
- Dromundo-Arias, O.A., and Peral-Carranza, H.D., 2007, Carta geológico-minera San Francisco de Asís G13–D31, Durango, México: Consejo de Recursos Minerales, escala 1:50,000, 1 sheet.
- Ferrari, L., López-Martínez, M., Aguirre-Díaz, G., and Carrasco-Núñez, G., 1999, Space-time patterns of Cenozoic arc volcanism in central Mexico: From the Sierra Madre Occidental to the Mexican volcanic belt: *Geology*, v. 27, p. 303–307.
- Ferrari, L., López-Martínez, M., and Rosas-Elguera, J., 2002, Ignimbrite flare-up and deformation in the southern Sierra Madre Occidental, western Mexico: Implications for the late subduction history of the Farallon plate: *Tectonic*, v. 21, p. 17–24.
- Ferrari, L., Valencia-Moreno, M., and Bryan, S., 2007, Magmatism and tectonics of the Sierra Madre Occidental and its relation with the evolution of the western margin of North America: *Geology Society of America Special Paper* 422, p. 1–39.
- Fisher, R.V., 1961, Proposed classification of volcanoclastic sediments and rocks: *Geological Society of America Bulletin*, v. 72, p. 1409–1414.
- 1984, Submarine volcanoclastic rocks: *Geological Society of London Special Publication* 16, p. 5–27.
- Fisher, R.V., and Schmincke, H.U., 1984, *Pyroclastic rocks*: Berlin Heidelberg New York Tokyo, Springer-Verlag, 472 p.
- Franco-Rubio, M., Comaduran-Ahumada, O., Alva-Valdivia, L.M., Urrutia-Fucugauchi, J., and Molina Garza, R.S., 2007, The Olivos olistostrome: Remnant of a late Permian oceanic basin along the southwestern margin of Laurentia, Chihuahua, Mexico: *International Geology Review*, v. 49, p. 1127–1144.
- Gemmell, J.B., Simmons, S.F., and Zantop, H., 1988, The Santo Niño silver-lead-zinc vein, Fresnillo district, Zacatecas, Mexico: Part I. Structure, vein stratigraphy, and mineralogy: *ECONOMIC GEOLOGY*, v. 83, p. 1597–1618.
- Gifkins, C.C., Allen, R.L., and McPhie, J., 2005, Apparent welding textures in altered pumice-rich rocks: *Journal of Volcanology and Geothermal Research*, v. 142, p. 29–47.
- Henry, C.D., and Aranda-Gómez, J.J., 1992, The real southern basin and range: Mid- to late Cenozoic extension in Mexico: *Geology*, v. 20, p. 701–704.
- Horner, J.T., and Enriquez, E., 1999, Epithermal precious metal mineralization in a strike-slip corridor: The San Dimas district, Durango, Mexico: *ECONOMIC GEOLOGY*, v. 94, p. 1375–1380.
- Ingram, R.L., 1954, Terminology for the thickness of stratification and parting units in sedimentary rocks: *Geology Society of America Bulletin*, v. 65, p. 937–938.
- Krapež, B., and Hand, J.L., 2008, Late Archean deep-marine volcanoclastic sedimentation in an arc-related basin: The Kalgoorlie Sequence of eastern Goldfields superterrane, Yilgarn craton, Western Australia: *Precambrian Research*, v. 161, p. 89–113.
- Lehmann, C., Osleger, D.A., Montañez, I.P., Sliter, W., Arnaud-Vanneau, A., and Banner, J., 1999, Evolution of Cupido and Coahuila carbonate plateforms, Early Cretaceous, northeastern Mexico: *Geological Society of America Bulletin*, v. 111, p. 1010–1029.
- Lorenz, V., 1986, On the growth of maars and diatremes and its relevance to the formation of tuff rings: *Bulletin of Volcanology*, v. 48, p. 265–274.
- Lowe, D.R., 1982, Sediment gravity flows: II. Depositional models with special reference to the deposits of high-density turbidity currents: *Journal of Sedimentary Petrology*, v. 52, p. 279–297.
- Ludwig, K.R., 2003, Mathematical-statistical treatment of data and errors for $\text{Th-}^{230}\text{U}$ geochronology: *Reviews in Mineralogy and Geochemistry*, v. 52, p. 631–656.
- Luhr, J.F., Henry, C.D., Housh, T.B., Aranda-Gómez, J.J., and McIntosh, W.C., 2001, Early extension and associated mafic alkaline volcanism from the southern Basin and Range province: Geology and petrology of the Rodeo and Nazas volcanic fields, Durango, Mexico: *Geology Society of America Bulletin*, v. 113, p. 760–773.
- Lyons, J.I., 1988, Geology and ore deposits of the Bolaños silver district, Jalisco, Mexico: *ECONOMIC GEOLOGY*, v. 83, p. 1560–1582.
- McDonald, A.J., Kreczmer, M.J., and Kesler, S.E., 1986, Vein, manto, and chimney mineralization at the Fresnillo silver-lead-zinc mine, Mexico: *Canadian Journal of Earth Sciences*, v. 23, p. 1603–1614.
- McDowell, F.W., and Clabaugh, S.E., 1979, Ignimbrites of the Sierra Madre Occidental and their relation to the tectonic history of western Mexico: *Geology Society of America Special Paper* 180, p. 113–124.

- McDowell, F.W., and Keizer, R.P., 1977, Timing of mid-Tertiary volcanism in the Sierra Madre Occidental between Durango City and Mazatlán, Mexico: *Geology Society of American Bulletin*, v. 88, p. 1479–1487.
- McPhie, J., Doyle, M., and Allen, R.L., 1993, *Volcanic textures: A guide to the interpretation of textures in volcanic rocks*: Tasmania, Center for Ore Deposit Research, University of Tasmania, Hobart, 198 p.
- Moller, S.A., Islas, J.E., and Davila, R.T., 2001, New discoveries in the La Colorada district, Zacatecas State, Mexico: *Society of Economic Geologists Special Publication 8*, p. 95–104.
- Munguía-Rojas, P., García-Padilla, J.L., Armenta Román, R., and Camacho, J.M., 2000, Carta geológico-minera Santiago Papasquiaro G13-8, Durango, México: Consejo de Recursos Minerales, escala 1:250,000, 1 sheet.
- Mutti, E., Tinterri, R., Benevelli, G., Di Biase, D., and Cavanna, G., 2003, Deltaic, mixed and turbidite sedimentation of ancient foreland basins: *Marine and Petroleum Geology*, v. 20, p. 733–755.
- Nieto-Samaniego, Á.F., Ferrari, L., Alaniz-Álvarez, S.A., Labarthe-Hernández, G., and Rosas-Elguera, J., 1999, Variation of Cenozoic extension and volcanism across the southern Sierra Madre Occidental volcanic province, Mexico: *Geological Society of America Bulletin*, v. 111, p. 347–363.
- North American Commission on Stratigraphic Nomenclature, 2005, *North American Stratigraphic Code*: American Association of Petroleum Geologists Bulletin, v. 89, p. 1547–1591.
- Pearce, J.A., and Peate, D.W., 1995, Tectonic implications of the composition of volcanic arc magmas: *Annual Review of Earth Planetary Sciences*, v. 23, p. 251–285.
- Pearson, M.F., Clark, K.F., Porter, E.W., and Gonzales S., O., 1988, Mineralogy, fluid characteristics, and silver distribution at Real de Ángeles, Zacatecas, Mexico: *ECONOMIC GEOLOGY*, v. 83, p. 1737–1759.
- Reading, H.G., 2002, *Sedimentary environments: Process, facies and stratigraphy*, 3rd ed.: Cambridge, Massachusetts, Blackwell Science, 688 p.
- Richards, M., and Bowman, M., 1998, Submarine fans and related depositional systems II: Variability in reservoir architecture and wireline log character: *Marine and Petroleum Geology*, v. 15, p. 821–839.
- Richards, M., Bowman, M., and Reading, H., 1998, Submarine-fan systems I: Characterization and stratigraphic prediction: *Marine and Petroleum Geology*, v. 15, p. 689–717.
- Richards, J.P., Wilkinson, D., and Ullrich, T., 2006, Geology of the Sari Gunay epithermal gold deposit, Northwest Iran: *ECONOMIC GEOLOGY*, v. 101, p. 1455–1496.
- Rubin, J.N., and Kyle, J.R., 1988, Mineralogy and geochemistry of the San Martín skarn deposit, Zacatecas, Mexico: *ECONOMIC GEOLOGY*, v. 83, p. 1782–1801.
- Ruvalcaba-Ruiz, D.C., and Thompson, T.B., 1988, Ore deposits at the Fresnillo mine, Zacatecas, Mexico: *ECONOMIC GEOLOGY*, v. 83, p. 1583–1597.
- Sillitoe, R.H., 1985, Ore-related breccias in volcanoplutonic arcs: *ECONOMIC GEOLOGY*, v. 80, p. 1467–1514.
- 1993, Epithermal models: Genetic types, geometric controls and shallow features: *Geological Association of Canada Special Paper 40*, p. 403–417.
- 1997, Characteristics and controls of the largest porphyry copper-gold and epithermal gold deposits in the circum-Pacific region: *Australian Journal of Earth Sciences*, v. 44, p. 373–388.
- 2010, Porphyry copper systems: *ECONOMIC GEOLOGY*, v. 105, p. 3–41.
- Sillitoe, R.H., and Bonham, H.F.J., 1984, Volcanic landforms and ore deposits: *ECONOMIC GEOLOGY*, v. 79, p. 1286–1298.
- Sillitoe, R.H., and Hedenquist, J.W., 2003, Linkages between volcanotectonic settings, ore-fluid compositions, and epithermal precious metal deposits: *Society of Economic Geologists Special Publication 10*, p. 315–343.
- Sparks, R.S.J., Self, S., and Walker, G.P.L., 1973, Products of ignimbrite eruption: *Geology*, v. 1, p. 115–118.
- Stewart, J.H., 1998, Regional characteristics, tilt domains, and extensional history of the late Cenozoic Basin and Range province, western North America: *Geological Society of America Special Paper 323*, p. 47–74.
- Sun, S.S., and McDonough, W.F., 1989, Chemical and isotopic systematics of oceanic basalts: Implications for mantle composition and processes: *Geological Society of London Special Publication 42*, p. 313–345.
- Swanson, E.R., Kempton, K.A., McDowell, F.W., and McIntosh, W.C., 2006, Major ignimbrites and volcanic centers of the Copper Canyon area: A view into the core of Mexico's Sierra Madre Occidental: *Geosphere*, v. 2, p. 125–141.
- Talling, P.J., Wynn, R.B., Masson, D.G., Frenz, M., Cronin, B.T., Schiebel, R., Akhmetzhanov, A.M., Dallmeier-Tiessen, S., Benetti, S., Weaver, P.P.E., Georgiopoulou, A., Zühlsdorff, C., and Amy, L.A., 2007, Onset of submarine debris flow deposition far from original giant landslide: *Nature*, v. 450, p. 541–544.
- Ulrich, T., Kamber, B.S., Jugo, P.J., and Tinkham, D.K., 2009, Imaging element-distribution patterns in minerals by laser ablation-inductively coupled plasma-mass spectrometry (LA-ICP-MS): *Canadian Mineralogist*, v. 47, p. 1001–1012.
- Wentworth, C.K., 1922, A scale of grade and class terms for clastic sediments: *Journal of Geology*, v. 30, p. 377–392.
- White, J.D.L., and Houghton, B.F., 2006, Primary volcanoclastic rocks: *Geology*, v. 34, p. 677–680.
- White, J.D.L., McPhie, J., and Skilling, I., 2000, Peperite: a useful genetic term: *Bulletin of Volcanology*, v. 62, p. 65–66.
- Wiedenbeck, M., Allé, P., Corfu, F., Griffin, W.L., Meier, M., Oberli, F., Von Quadt, A., Roddick, J.C., and Spiegel, W., 1995, Three natural zircon standards for U-Th-Pb, Lu-Hf, trace element and REE analyses: *Geostandards and Geoanalytical Research*, v. 19, p. 1–23.
- Wilson, C.J.N., and Walker, G.P.L., 1982, Ignimbrite depositional facies: the anatomy of a pyroclastic flow: *Journal of Geological Society of London*, v. 139, p. 581–592.
- Yuan, H.L., Gao, S., Liu, X.M., Li, H.M., Günther, D., and Wu, F.Y., 2004, Accurate U-Pb age and trace element determinations of zircon by laser ablation inductively coupled plasma-mass spectrometry: *Geostandards and Geoanalytical Research*, v. 28, p. 353–370.
- Zawada, R.D., Albinson, T., and Abeyta, R., 2001, Geology of the El Crestón gold deposit, Sonora State, Mexico: *Society of Economic Geologists Special Publication 8*, p. 187–197.



Chapter X

Appendix

The La Pitarrilla Silver-Zinc-Lead Deposit, Sierra Madre Occidental, Mexico: A Description of the Mineralization and a Reconstruction of Its Volcano-Sedimentary Environment

CLAIRE M. J. SOMERS,[†] HAROLD L. GIBSON, AND RON BURK

The Appendix contains detailed descriptions of volcanic and sedimentary lithofacies and intrusions that host the Ag-Zn-Pb mineralization at La Pitarrilla.

Terminology

Two, nongenetic granulometric-based nomenclatures are used here to describe and classify clastic volcanic and sedimentary rocks at La Pitarrilla. Herein, the term volcanoclastic is used to describe a clastic rock composed entirely or dominantly (>60%) of volcanic material and may include primary autoclastic (including hyaloclastite), pyroclastic, and peperitic deposits, and their redeposited, syneruptive equivalents (White and Houghton, 2006). As many primary and resedimented volcanoclastic deposits are difficult to distinguish, these deposits are classified using the same nongenetic terms that are based on the size and percentage of clasts (material >2 mm in size) relative to matrix (material <2 mm) into tuff, lapilli tuff, lapillistone, and tuff breccia as proposed by Fisher (1961) and White and Houghton (2006). The term sedimentary is used to describe epiclastic terrigenous and chemical sedimentary rocks; the former refers to rocks composed exclusively to dominantly (>60%) of material derived through chemical or mechanical weathering. Sedimentary lithofacies are classified according to the percentages of gravel, sand, silt, and clay-sized particles, as defined by Wentworth (1922). Bed-thickness terminology for both the volcanoclastic and sedimentary lithofacies is in accordance with the nomenclature proposed by Ingram (1954). Particulate gravity flows refer to all mixtures, in varying proportions, of water and sedimentary and/or volcanic particles as proposed by Reading (2002), and include low- and high-density turbidity currents and cohesive debris flows, some of which may have been eruption fed. The term ignimbrite is used to describe pumiceous pyroclastic flows irrespective of the degree of welding or volume, as defined by Sparks et al. (1973). Pyroclastic surge deposits refer to thin, fine-grained, well-sorted, and cross-stratified deposits (Fisher and Schmincke, 1984; Cas and Wright, 1987). Pyroclastic surge deposits are associated with ignimbrite eruptions and typically form by the collapse of the eruption cloud above the pyroclastic flow (ash cloud surge deposits) or through direct blasts from the ignimbrite flow front during explosive expansion of the flow head due to ingestion of air at the front lobes and clefts of the flow (ground surge deposits; Wilson and Walker, 1982).

[†] Corresponding author: e-mail, cm_somers@laurentian.ca

Lithofacies Description and Interpretation

In the following descriptive sections, lithofacies identified within each informal formation and member are described in stratigraphic order, i.e., from oldest to youngest, with reference to an idealized stratigraphic section in Figure 2. The distributions of the formations, members, and lithofacies are illustrated in Figures 3, 4, and 5. Unless otherwise stated, the composition of clasts, flows, and intrusions are based on representative analyses of least altered samples and field and petrographic observations of their mineralogy, textures, and structures. For example, clasts with quartz and feldspar phenocrysts or with only quartz phenocrysts are referred to as rhyolite; those with only feldspar phenocrysts are referred to as dacite; those with varying combinations of feldspar, amphibole, biotite, and pyroxene phenocrysts are referred to as andesite. Matrix refers to components less than 2 mm in diameter and estimates of matrix composition are based on color and mineralogy. Details regarding strata thickness, internal organization, clast composition and proportion, clast shape, and matrix composition for each member and lithofacies are contained in [Table A1](#).

Peña Ranch formation

Strata of the Peña Ranch formation form the Cretaceous basement to the predominantly Tertiary volcanoclastic and pyroclastic rocks and are best exposed in the low-lying area northeast of La Pitarrilla (Figs. 2–5). The Peña Ranch formation is dominated by folded and foliated lithofacies that were folded during the Laramide orogeny. These lithofacies consist of interbedded mudstone and siltstone with occasional beds of sandstone and pebble conglomerate that contain micritic limestone, vein quartz, heterolithic volcanic, and interbedded mudstone and siltstone clasts supported in a silt- to sand-sized matrix (Table A1; [Fig. A1A, B](#)). Beds of thinly to very thickly bedded micritic limestone are restricted to the northwestern corner of the map area (Figs. 3, A1C). Strontium isotopic analyses of two samples collected from limestone beds yielded $^{87}\text{Sr}/^{86}\text{Sr}$ ratios of 0.70745 ± 0.00001 , which are similar to those obtained for late Albian limestones located in the Coahuila block of northeastern Mexico (Lehmann et al., 1999) and are consistent with late Albian seawater (Bralower et al., 1997).

The absence of bed forms indicative of wave- or tide-formed structures produced in shallow marine environments suggests that the Peña Ranch formation was deposited below

TABLE A1. Summary of Each Formation (Fm), Member, and Lithofacies at the La Pitarrilla Ag-Zn-Pb Deposit

Fm	Member/ Lithofacies	Thickness	Internal organization	Clast proportion, shape and type	Matrix
Pena Ranch		Undetermined	(1) Mud and silt: TnL to TL, interbedded, cross-bedded, rip-up clasts, boudinage of beds, foliated (2) Conglomerate: MB to VTB, heterolithic, unsorted, matrix-supported, locally stratified, increase in abundance at upper contact	(2) Proportion: 75 to 80% Shape: Rounded to sub-angular Type: Lim, MP, aphyric, FP, QP, and QFP, qz ± mud, silt	(2) Silt- to sand-sized with 15% qz, 1% musc, and 1% plag
	Manto Rico member	3-90 m	2 heterolithic and matrix-supported lithofacies: - Poorly sorted, pebble to cobble conglomerate: VTB - Crudely stratified, granule to cobble conglomerate: MB to VTB, lim clasts aligned parallel to bedding T beds: TL to VTB, normally graded or massive LPS beds: (1) a heterolithic facies and (2) a monolithic facies	Proportion: 40 to 60% Shape: Angular ± irregularly shaped; angular Type: Lim, silt, mud ± AP; aphyric, fb, calc vein	Sand-sized with 2% qz
	Lower member	4-42 m		(1) Proportion: 80 to 100% Shape: Irregularly shaped ± sub-rounded to angular Type: AP ± mud, silt, FP, aphyric (2) Same than (1), but only with AP clasts	Tuff-sized with 3% qz and 3% amph
	Middle member				
Pitarrilla	Heterolithic lithofacies	17-173 m	TBx: VTB, heterolithic, matrix-supported, poorly sorted, intercalated with LPS and T (similar to Lower Member) LPT and LPS: MB to TB, heterolithic, matrix-supported, normal grading with lesser inverse grading	Proportion: 40% for TBx; 40 to 75% for LPT and LPS Shape: Sub-angular to angular Type: Aphyric, FP, AFP, AP	Tuff-sized with 20% fld (plag + K-fld), 5% qz, and local 1 to 5% musc
	Tuff lithofacies	4-28 m	(1) VTB tuff (2) TnL to TnB tuff with normal graded bed and erosive contact	(1) Proportion: 10% Shape: Sub-rounded to angular Type: Aphyric (2) Too fine to determine	(1) 10% fld (plag + K-fld), 5% qz, and 2% musc strongly clay-altered within finer-grained matrix (2) 2% qz shards
	Flow lithofacies	46-171 m	2 facies: (1) Coherent massive facies: light grey-green to cream color due to argillic alteration, aphanitic, homogeneous except for the occasional fb (2) Monolithic breccia facies: restricted to margin of lithofacies	(2) Proportion: 30 to 40% Shape: Angular, platy, and cusped (shards) Texture: Jigsaw-fit, clast-rotated Size: LPT to TBx Type: Coherent massive facies	(1) Microcrystalline feldspar groundmass with minor clay-altered mafic phenocrysts (2) Shard-rich hyaloclastite with 2% qz and 1% fld
	Lapilli tuff lithofacies	20-112 m	2 heterolithic facies: (1) Non-bedded facies: poorly sorted, framework-supported towards the lower contact and grades upward to a matrix-supported lapilli tuff (2) Interbedded T and LPT facies: MB to TB	Proportion: 35 to 50% (1) Shape: Rounded ± irregularly shaped; angular Type: FAP ± FP; silt (2) Shape: Sub-rounded to rounded Type: FAP, AP, BFP ± FAPP, PFP	(1) Tuff-sized with 10% fld (plag + K-fld), 3 to 5% qz, and 2% musc (2) Tuff-sized with 5% qz, 3% musc, and 1 to 3% fld (K-fld + rare plag)
	Upper member	30-68 m	MB to TB, heterolithic, matrix-supported, contain limestone clasts that are dark grey on fresh surfaces and weather to a brownish color	Proportion: 25 to 75% Shape: Sub-rounded to rounded, angular Type: FAP, BFP, AP, lim	Identical to interbedded LPT and T facies of lapilli tuff lithofacies
	Lithic-rich tuff and lapilli tuff lithofacies	30-112 m	Lithic T: VTB, locally qz-rich, fld-rich, lithic-rich or qz- and lithic-rich, grade from framework-supported at the base of beds to matrix-supported at the top of beds Lithic LPT: TB to VTB, locally framework-supported at the base	Proportion: 15 to 40 % Shape: Elongated and wispy, rounded to angular and irregular shaped Type: Pumice (?), mud, silt, AFP, AP, FP, QFP, BFP, QP, and lithic-rich tuff and lapilli tuff lithofacies	Clay-altered groundmass with 5 % qz ex shards, 3 % fld (K-fld + rare plag), and local 2 % bio Locally rich in qz (30 to 40 %) or fld (15 %)
Cardenas					

TABLE 1. (Continued)

Fm	Member/ Lithofacies	Thickness	Internal organization	Clast proportion, shape and type	Matrix
Cardenas	Crystal- rich pumice tuff lithofacies	17-106 m	2 facies: (1) Crystal- and pumice-rich tuff facies: Massive, eutaxitic texture, columnar joint, 2 to 5% of lithic clasts toward the base (2) Stratified facies: TnL to TL, well-stratified and cross-stratified, columnar joint	(1) Proportion: 22 to 25% Shape: Elongated and wispy ± sub-rounded to angular Type: QFP long-tube pumice ± FP, QFP, aphyric, mud, lapilli tuff lithofacies (2) Proportion, shape, and type: Clasts strongly clay-altered and in majority leached	(1) Clay altered microcrystalline qz groundmass with 10% qz and 5% K-fld and cx shards, local 1% bio (2) Tuff-sized with 2% qz
	Stratified tuff lithofacies	(1) 0.1-0.3 m (2) 1-15 m	(1) Lapillistone facies: (A) Matrix-supported and monolith lithic lapillistone; (B) Framework-supported and heterolith lithic lapillistone (2) Stratified tuff lithofacies: Well-sorted and -stratified, TnL to TL beds, local cross-bedding, locally interbedded with the overlying lithic-rich tuff lithofacies	(1) Proportion: (A) 50%; (B) 90% Shape: (A) Angular; (B) Sub-rounded to angular ± sub-angular to angular Type: (A) Aphyric; (B) Perlitic and aphyric ± FP, FMP, MP, QP, mud (2) Proportion: 45 to 50% Shape: Angular ± rounded, irregularly shaped Type: Perlitic and aphyric ± MP, FP, silt	(1) (A) Tuff-sized (B) Tuff-sized with 1% qz (2) Tuff-sized with 2% qz and 2% fld (probably K-fld)
	Lithic-rich tuff lithofacies	0.8-10 m	Heterolith lithic, matrix-supported, massive, TB to VTB	Proportion: 5 to 1% Shape: Elongated and wispy, rounded to angular Type: Pumice (?), aphyric, FP, silt	Clay-altered groundmass with 5% qz cx shards and 2% K-fld
	Lower volcaniclastic lithofacies	7-25 m	Non-bedded, poorly sorted	Proportion: 25% Shape: Rounded to angular ± irregularly shaped Type: FP, FMP ± aphyric	Tuff-sized with 30% fld
Casas Blancas	Upper volcaniclastic lithofacies	15-160 m	2 heterolith lithic facies: (1) T and LPS facies: MB to TB, normal and inversely graded (2) Non-bedded LPS to TBx facies: poorly sorted	Proportion: (2) 25 to 75% Shape: Rounded to angular Type: Encino dome lithofacies ± aphyric, fb, FP, QP, MP, lithic-rich tuff and lapilli tuff lithofacies	Tuff-sized with 5% qz and fld
	Encino dome lithofacies	85-100 m	Coherent, local breccia and columnar joint, fb varies from sub-horizontal at basal contact to vertical within dome interior	Textures at the base: Hyaloclastite, lithophysae, perlitic fractures, spherulites	Microcrystalline qz groundmass with 3% K-fld and 2% qz
Intrusions	Lower mafic sill	80-110 m	(1) Coherent massive facies; (2) Peperite facies along the margins	(2) Proportion: 20 to 50% Shape: Irregularly shaped ± angular to sub-rounded Type: AP ± Lower member, Middle member	(1) Microcrystalline plagioclase groundmass with 15% amphi
	Felsic Intrusions (A) Dikes (B) Sill	(A) 2-44 m (B) 10- 128 m	(1) Coherent facies: Massive within interior, but fb along and parallel to margins (2) Peperite along the margins with Pitarrilla, Casas Blancas, and rarely Peña Ranch formations	(2) Proportion: 25 to 95% Shape: Irregularly shaped ± angular to sub-rounded Type: QFP ± Pitarrilla formation, Casas Blancas formation, Peña Ranch formation	(1) Microcrystalline qz groundmass with 3% K-fld and 2% qz
	Upper mafic sill	2-53 m	(1) Coherent massive sill (2) Local peperite within sill	(2) Proportion: 50 to 80% Shape: Irregularly shaped ± elongated rounded Type: AP ± upper volcaniclastic lithofacies member	(1) Microcrystalline plagioclase groundmass with 20% amphi and 1% olv

Crystals abbreviations: Amph = amphibole, bio = biotite, calc = calcite, cx = crystals, fld = feldspar, fld = olivine, plagi = plagioclase, qz = quartz, **Sedimentary class abbreviations:** Lim = limestone, mud = mudstone, silt = siltstone; **Composition class abbreviations:** AFP = amphibole-feldspar-phryic clast, AP = amphibole-phryic clast, BFP = biotite-feldspar-phryic clast, FMP = feldspar-mafic-phryic clast, FAP = feldspar-phryic clast, FPP = feldspar-amphibole-phryic clast, FAPP = feldspar-amphibole-pyroxene-phryic clast, MP = mafic-phryic clast, PFP = pyroxene-feldspar-phryic clast, QFP = quartz-feldspar-phryic clast, QP = quartz-phryic clast; **Clasts textures abbreviations:** Fb = flow-banded clasts; **Bedding thickness abbreviations:** MB = medium bedded, TB = thickly bedded, TL = thickly bedded, T = tuff, TBx = tuff breccia
End-member rock term abbreviations: LPT = lapilli-tuff, LPS = lapillistone, T = tuff, TBx = tuff breccia

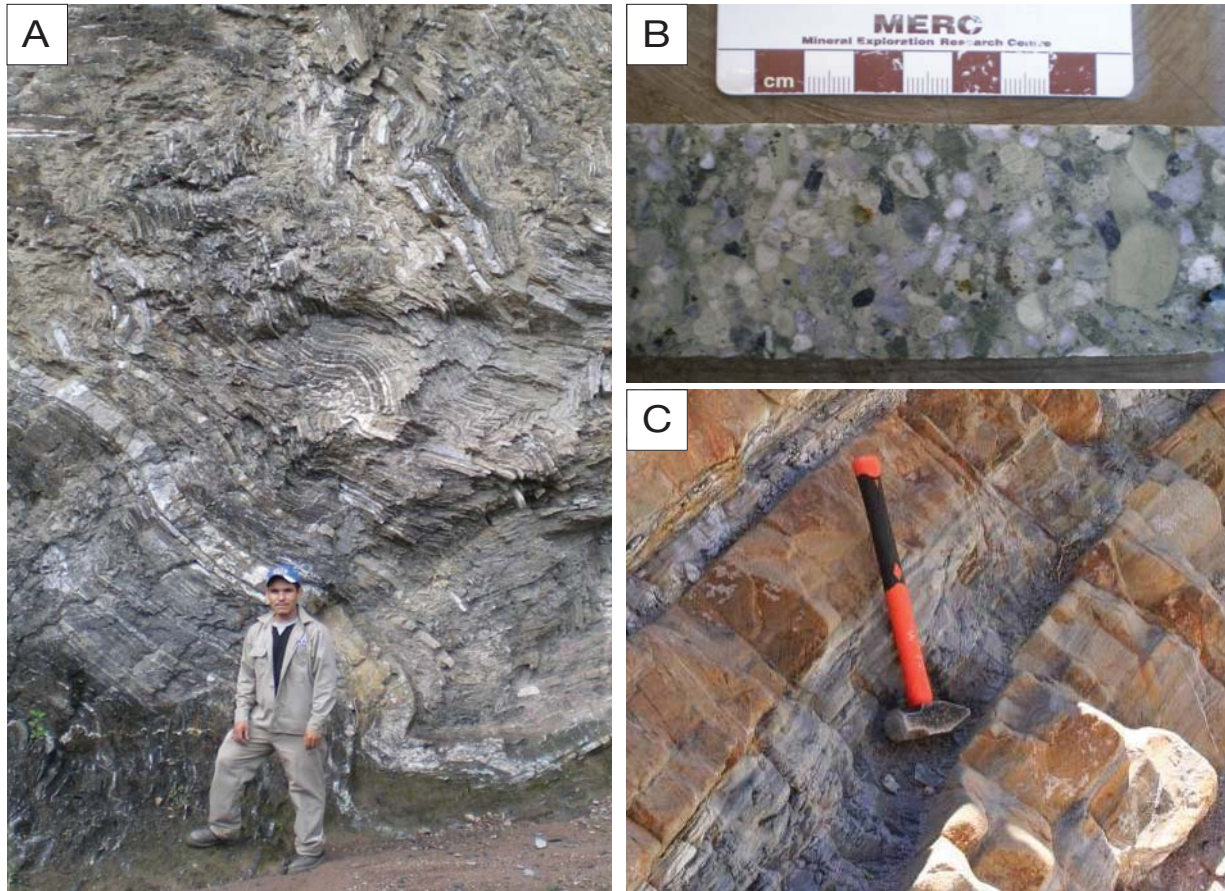


FIG. A1. Lithofacies of the Peña Ranch formation. A. Folded interbedded mudstone and siltstone beds. B. Clast-supported heterolithic pebble conglomerate bed with volcanic, quartz, and interbedded mudstone and siltstone clasts. C. Interbedded mudstone, siltstone, and carbonate beds (orange) that are located in the northwest corner of the map area.

storm wave base and within a marine environment. The close association of sand to pebble conglomerate lithofacies with mudstone and siltstone lithofacies as indicated by their intercalation and the occurrence of interbedded mudstone and siltstone clasts, interpreted to be ripup clasts, suggests depositional processes characterized by rapid fluctuations in depositional rate and sedimentary grain size coupled with erosional scour (e.g., Krapež and Hand, 2008). The sand to pebble conglomerate lithofacies was most likely deposited from gravelly high-density turbidity currents, whereas the interbedded mudstone and siltstone lithofacies were deposited from low-density turbidity currents (e.g., Lowe, 1982). The Peña Ranch formation is interpreted to be the stratigraphic equivalent of the Cretaceous Mezcalera Formation. It hosts a significant part of the sulfide-associated mineralization at La Pitarrilla.

Pitarrilla formation

The Pitarrilla formation unconformably overlies the Peña Ranch formation and consists of four members which, from oldest to youngest, are the Manto Rico, Lower, Middle, and Upper members (Table A1; Figs. 2–5).

The Pitarrilla formation is interpreted to have been deposited below storm wave base and within a marine environment. This is based on the absence of cross stratification and

erosional scour indicative of an alluvial-fluvial environment, the absence of bed forms indicative of wave- or tide-formed structures produced in shallow marine environment, and the occurrence of interbedded turbidites, which are characteristic of deep-marine clastic environments.

Manto Rico member: The Manto Rico member unconformably overlies the Peña Ranch formation (Figs. 2–5) and is characterized by abrupt lateral variations in thickness (Table A1), which suggests channelized deposition. This member consists of two lithofacies, a poorly sorted, pebble to cobble conglomerate, and a crudely stratified, granule to cobble conglomerate (Table A1; Fig. A2A). Both lithofacies contain distinctive tabular clasts of micritic limestone, angular clasts of terrigenous sedimentary rocks, and irregularly shaped andesitic volcanic clasts in a sand-sized matrix (Table A1; Fig. A2A). The micritic limestone clasts are petrographically similar to the limestone beds of the underlying Peña Ranch formation. The andesitic clasts are petrographically identical to those within the overlying Lower member.

The poor sorting, the dominantly massive, the thickly bedded character, and the presence of a sandy matrix suggest that the pebble to cobble conglomerate lithofacies was deposited from cohesive debris flows (Lowe, 1982), whereas the granule to cobble conglomerate is characteristic of deposits derived from gravelly high-density turbidity currents (Lowe,

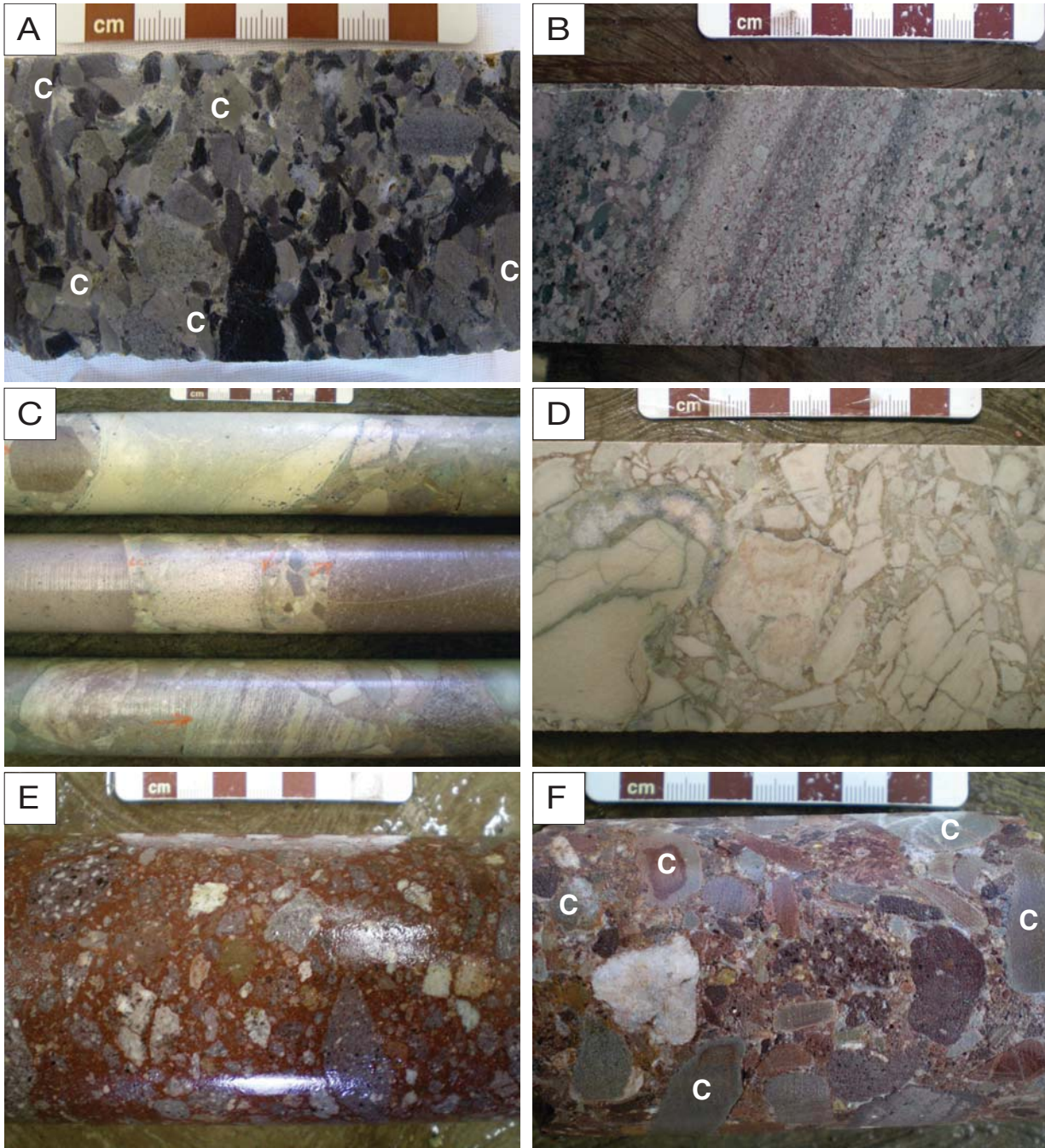


FIG. A2. Members and lithofacies of the Pitarrilla formation. A. Very thickly bedded and clast-supported heterolithic pebble conglomerate of the Manto Rico member composed of tabular carbonate clasts (C) and angular clasts of terrigenous sedimentary rocks. B. Well-stratified and clay-altered Lower member, which consists of interbedded lapillistone and tuff beds that are thinly laminated to thinly bedded and are composed of irregularly shaped andesitic clasts. C. Very thickly bedded, poorly sorted, clay-altered tuff-breccia of the heterolithic lithofacies within the Middle member that contains angular dacitic and andesitic volcanic clasts in a tuff-sized matrix. D. Clay-altered autoclastic flow breccia of the flow lithofacies within the Middle member that consists of monolithic, angular clasts with a jigsaw-fit texture that range from lapilli to block size within a tuff-sized, hyaloclastic matrix. E. Lapilli tuff bed of the interbedded tuff and lapilli tuff facies of the Middle member that contains subrounded to rounded dacitic and andesitic clasts supported by a tuff-sized matrix. F. Lapilli tuff bed of the Upper member that contains subrounded to rounded dacitic and andesitic clasts, and gray-colored tabular carbonate clasts (C) within a tuff-sized matrix.

1982). The clasts of siltstone and mudstone are interpreted to have been derived from identical lithofacies found in the underlying Peña Ranch formation. The source of the andesitic

volcanic clasts is uncertain; however, their irregular delicate shape is suggestive of a pyroclastic origin. If so, then the absence of vesicles indicates fragmentation by hydrovolcanic

eruptions (Fisher and Schmincke, 1984) and their derivation from primary, unconsolidated pyroclastic deposits. Their occurrence with limestone and terrigenous sedimentary clasts indicates transport and redeposition of the andesitic clasts from their original source. The Manto Rico member is the most economically important ore host at the La Pitarrilla deposit.

Lower member: The Lower member conformably overlies the Manto Rico member (Figs. 2–5) and is characterized by irregularly shaped andesitic clasts, identical to those found in the Manto Rico member, within a tuff-sized matrix (Table A1). This member consists of interbedded lapillistone and tuff beds (Table A1; Fig. A2B). The lapillistone beds are divisible into two facies that occur separately or are interbedded. These facies include a heterolithic facies, where the dominant andesitic clasts are mixed with a minor component (5–25%) of subrounded to angular clasts of terrigenous sedimentary rocks and rounded volcanic clasts, and a monolithic facies containing only the andesitic clasts (Table A1).

Based on grain-size populations for low- and high-density turbidity currents (Lowe, 1982), the lapillistone beds are interpreted to have been deposited from high-density turbidity currents, whereas the tuff beds were deposited from low-density turbidity currents. The intercalation of lapillistone and tuff beds is consistent with deposition from multiple low- and high-density turbidity currents, which could have resulted from the initial deposition from a high-density turbidity current followed by deposition from a residual low-density current mainly composed of tuff-sized material (Lowe, 1982). Sparse clasts of siltstone and mudstone are interpreted to be derived from the underlying Peña Ranch formation. The andesitic volcanic clasts are identical to those found in the Manto Rico member and probably share the same or a similar pyroclastic provenance and subsequent transport and redeposition history. The only difference is that the monolithic facies may be a product of direct redeposition from a primary pyroclastic deposit without incorporation of components derived from the Cretaceous sedimentary basement during transport. Alternatively, the monolithic facies could be a primary pyroclastic deposit.

Middle member: The Middle member of the Pitarrilla formation conformably overlies the Lower member and is comprised of three volcanoclastic lithofacies and one flow lithofacies (Fig. 2). From oldest to youngest, these include the heterolithic lithofacies, the tuff lithofacies, the flow lithofacies, and the lapilli tuff lithofacies (Table A1; Figs. 2–5).

Heterolithic lithofacies: The heterolithic lithofacies consists of tuff breccia, intercalated with tuff and lapillistone, and overlain by interbedded lapilli tuff and lapillistone (Table A1; Figs. 2, 4, 5). The tuff breccia contains subangular to angular dacitic and andesitic clasts that are supported by a tuff-sized matrix (Table A1; Fig. A2C). On a primitive mantle normalized multielement plot, clasts of the tuff breccia show negative Nb, Ta, and Ti anomalies and have a steep rare earth element (REE) pattern, all of which are indicative of calc-alkaline, arc volcanism (Pearce and Peate, 1995; Fig. A3A). The interbedded tuff and lapillistone is composed of irregularly shaped andesitic clasts within a tuff-sized matrix and is comparable to tuffs and lapilli tuffs of the Lower member (Table A1). The overlying lapilli tuff and lapillistone contain

angular dacitic and andesitic clasts within a tuff-sized matrix that is identical to the matrix of the underlying tuff breccia (Table A1).

The poor sorting with respect to clast composition and size, the massive nature, the matrix support, and the tuff-sized matrix suggest that the tuff breccia was deposited from cohesive debris flows (Lowe, 1982). The interbedded tuff and lapillistone are very similar to tuffs and lapillistones of the Lower member and represent deposits from multiple low- and high-density turbidity currents, whereas each cohesive debris flow deposit represents one event. The overlying lapilli tuff and lapillistone, based on the common occurrence of normal graded beds and the lapilli tuff and lapillistone grain size, are interpreted to have been deposited from multiple high-density turbidity currents (Lowe, 1982). The angular shape of the volcanic clasts, the lack of weathered rinds on the clasts, and the preservation of feldspar and muscovite crystals in the matrix are consistent with a proximal source of detritus derived either from unconsolidated subaerial or subaqueous volcanoclastic deposits or flows with a calc-alkaline arc signature.

Tuff lithofacies: The tuff lithofacies conformably overlies the heterolithic lithofacies and consists of a very thickly bedded tuff and a thinly laminated to thinly bedded tuff that occur interbedded or separately and both contain submillimeter lithic clasts and crystals (Table A1).

The absence of grading and the poorly defined stratification of the thickly bedded tuff are characteristic of a massive deposit emplaced without laminar or turbulent flow, whereas the well-stratified tuff is interpreted to be a product of low-density turbidity currents. Possible provenances for the well-stratified tuff include redeposition of primary pyroclastic deposits or a derivation through elutriation of fines during the emplacement of particulate gravity flows.

Flow lithofacies: The flow lithofacies conformably overlies and is locally overlain by the tuff lithofacies. It consists of two facies, a coherent massive facies that is overlain and locally underlain by a breccia facies that contains angular monolithic clasts of the coherent massive facies supported within a shard-rich, hyaloclastic matrix (Table A1; Fig. A2D). The contacts between the two facies are gradational. The coherent massive facies is andesitic in composition and has pronounced negative Nb, Ta, and Ti anomalies, and a steep REE pattern on primitive mantle normalized plots, which are typical of calc-alkaline arc andesites (Fig. A3B).

The monolithic nature of the clasts within the breccia facies, their angularity, jigsaw-fit texture, their gradation into the coherent massive facies, and their occurrence within a hyaloclastic matrix indicate that the breccia facies is an autoclastic flow breccia. The hyaloclastic matrix is interpreted to be a product of quench fragmentation of the magma during interaction with water (Batiza and White, 2000), which indicates emplacement of the flow within a subaqueous environment and is consistent with the interpreted subaqueous depositional environment for clastic lithofacies of the Pitarrilla formation.

Lapilli tuff lithofacies: The lapilli tuff lithofacies conformably overlies the flow lithofacies and include a nonbedded facies that is conformably overlain by a tuff and lapilli tuff facies (Table A1). The nonbedded facies contains rounded andesitic clasts with a minor component (5–10%) of irregu-

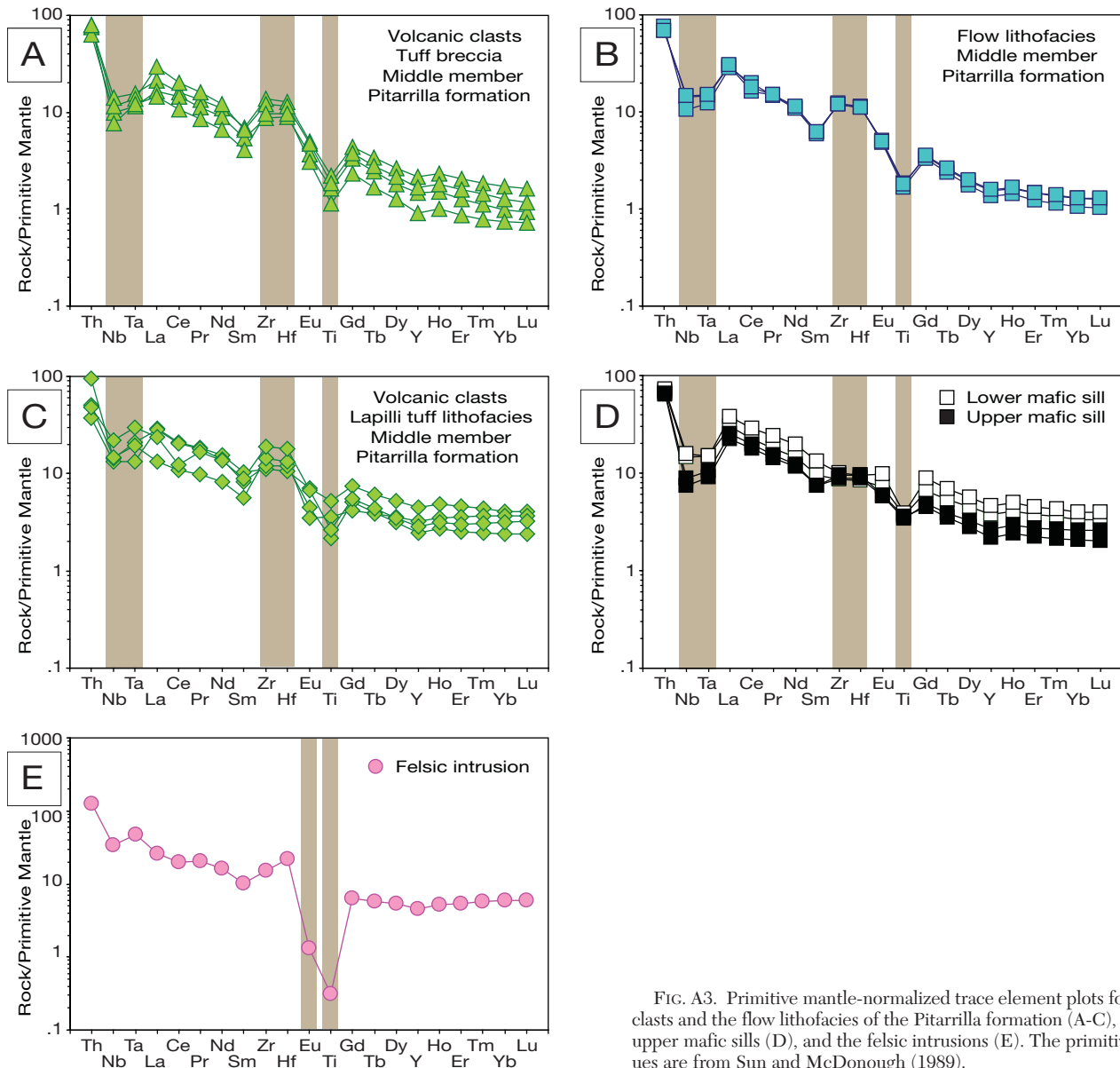


FIG. A3. Primitive mantle-normalized trace element plots for the volcanic clasts and the flow lithofacies of the Pitarrilla formation (A-C), the lower and upper mafic sills (D), and the felsic intrusions (E). The primitive mantle values are from Sun and McDonough (1989).

larly shaped dacitic clasts and angular clasts of terrigenous sedimentary rocks that are supported by a tuff-sized matrix (Table A1). The interbedded tuff and lapilli tuff facies is composed of subrounded to rounded dacitic and andesitic clasts within a tuff-sized matrix containing subrounded crystals (Table A1; Fig. A2E). On a primitive mantle normalized multi-element plot, andesitic clasts of the interbedded tuff and lapilli tuff facies display negative Nb, Ta, and Ti anomalies, and a moderately steep REE pattern, typical of arc volcanic rocks (Fig. A3C).

The poor size sorting, the massive nature, and the matrix-supported character of the nonbedded facies are characteristics of cohesive debris flows (Lowe, 1982). The local occurrence of an upper stratified facies may be the product of localized turbulence within the upper part of a particulate gravity flow during transport, which is typical of submarine cohesive debris flows undergoing flow transformation

(Fisher, 1984; Mutti et al., 2003; Talling et al., 2007). The arc affinity of the andesitic clasts suggests their derivation from unconsolidated arc volcanoclastic deposits. The irregularly shaped dacitic clasts share a similar morphology with andesitic clasts found in the Manto Rico and Lower members that suggests they may also be primary pyroclasts produced by hydrovolcanic eruptions that were redeposited. The subrounded to rounded form of the andesitic volcanic clasts and crystals within the interbedded tuff and lapilli tuff facies suggest a more significant transport distance and/or reworking for this facies than for the nonbedded facies. The stratified facies possesses a wider range of clast types than the nonbedded facies, which suggests a larger and/or more diversified provenance. The angular siltstone clasts are considered to be derived from siltstones of the Peña Ranch formation.

Upper member: The Upper member of the Pitarrilla formation conformably overlies the Middle member (Table A1;

Figs. 2–5) and consists of a well-stratified heterolithic lithofacies, identical to the interbedded tuff and lapilli tuff facies of the underlying lapilli tuff lithofacies, except for the presence of subrounded to tabular limestone clasts in the former (Table A1; Fig. A2F). The limestone clasts are identical in texture and color to limestone clasts found in the underlying Manto Rico member and to limestone beds in the Peña Ranch formation.

The Upper member is interpreted to be the product of sedimentation from high-density turbidity currents. The angular shape of the volcanic clasts and the preservation of feldspar and muscovite crystals in the matrix are consistent with a derivation from unconsolidated subaerial or subaqueous arc volcanoclastic deposits or flows.

Cardenas formation

The Cardenas formation unconformably overlies the Pitarilla formation and consists of four distinctive lithofacies

which, from oldest to youngest, are the lithic-rich tuff and lapilli tuff lithofacies, the crystal-rich pumice tuff lithofacies, the stratified tuff lithofacies, and the lithic-rich tuff lithofacies (Table A1; Figs. 2–5).

Lithic-rich tuff and lapilli tuff lithofacies: The lithic-rich tuff and lapilli tuff lithofacies unconformably overlies the Pitarilla formation, but its extent is limited compared to the overlying lithofacies of the Cardenas formation. The lithic-rich tuff and lapilli tuff lithofacies consists of lithic tuff intercalated with 20 percent lithic lapilli tuff. The former contains subangular to angular clasts of terrigenous sedimentary rocks and rounded to subangular volcanic clasts with a minor component (5%) of elongate, wispy, aphyric, clay-altered clasts; whereas the latter is composed of abundant (30%) elongate, wispy, aphyric clay-altered clasts and a similar abundance of lithic clasts (Table A1; Fig. A4A). Both lithofacies are supported by a strongly clay altered groundmass (Table A1). The

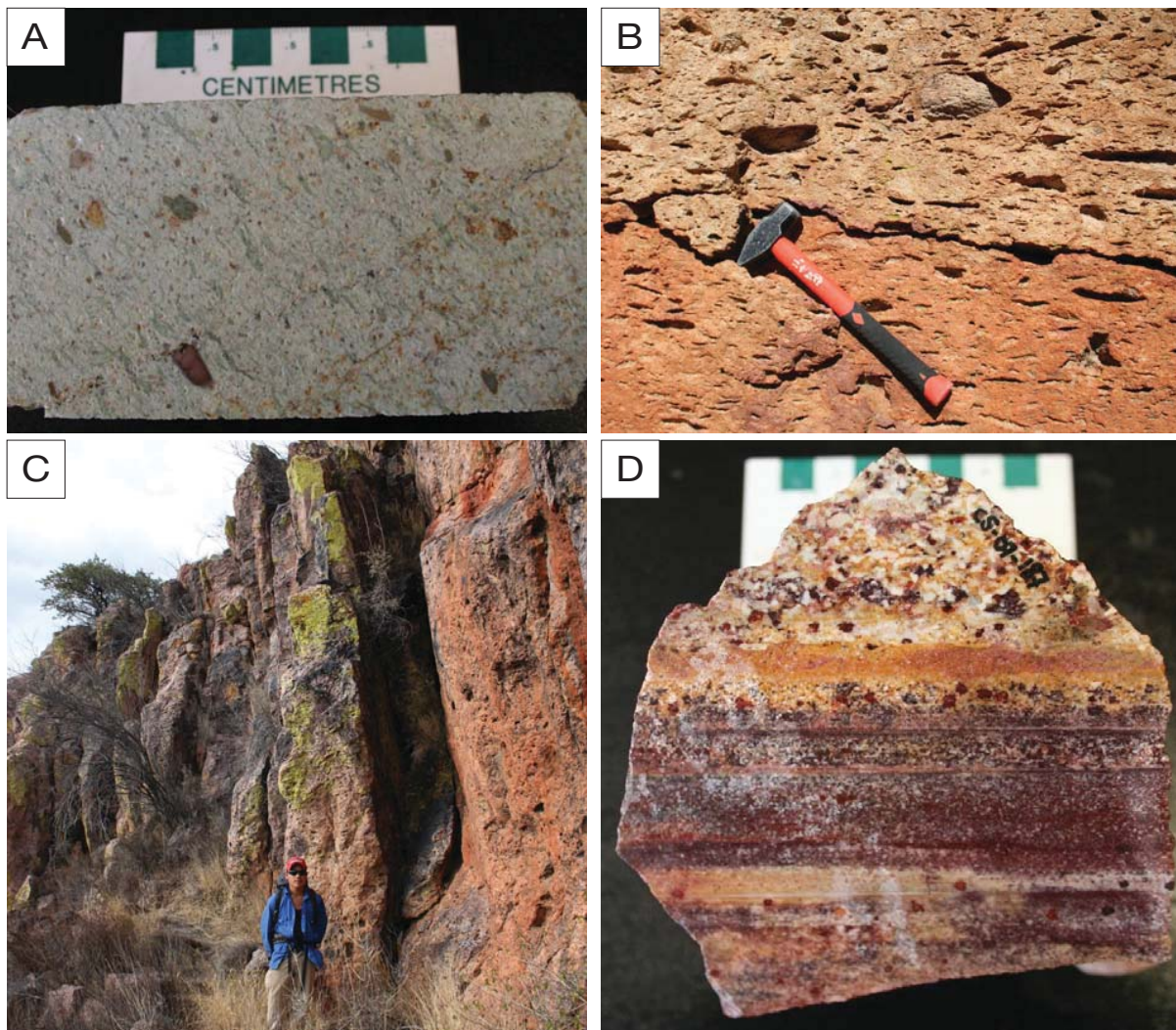


FIG. A4. Lithofacies of the Cardenas formation. A. Matrix-supported lapilli tuff of the lithic-rich tuff and lapilli tuff lithofacies that is characterized by abundant elongate, wispy, aphyric clay-altered pumice (?) clasts with a minor component of rounded to subangular volcanic clasts in a strongly clay altered matrix. Note the wispy clasts that define a planar fabric. B. Eutaxitic texture defined by flattened pumice clasts within clay- and limonite-altered crystal- and pumice-rich tuff facies of the crystal-rich pumice tuff lithofacies. C. Columnar joints within the crystal- and pumice-rich tuff facies of the crystal-rich pumice tuff lithofacies. E. Hematite-altered stratified tuff lithofacies containing well-sorted, thinly to thickly laminated tuff.

mudstone and siltstone clasts are similar to lithofacies found in the underlying Cretaceous sediments, and the dacitic and andesitic clasts are similar to those described in the volcanoclastics of the Pitarrilla formation. The wispy clasts define a planar fabric within the lapilli tuff beds that ranges from almost bedding-parallel to inclined by as much as 50° to depositional surfaces (Fig. A4A).

The elongate and wispy shape of the altered, aphyric clasts are characteristics of flattened vitric or pumice clasts, although the high degree of clay alteration precludes a definitive interpretation. If the wispy clasts are pumice, then the directional planar fabric could be a eutaxitic foliation that typically develops in incipiently welded to welded ignimbrites (Fisher and Schmincke, 1984), in which case the lithic-rich tuff and lapilli tuff lithofacies may represent multiple ignimbrites. Alternatively, the planar fabric, especially in altered rocks such as these, could result from the alteration, dissolution, and mechanical compaction of cold, pumice (vitric) clasts during lithification and diagenesis of either primary pyroclastic flow deposits or their redeposited equivalents (Gifkins et al., 2005).

Crystal-rich pumice tuff lithofacies: The crystal-rich pumice tuff lithofacies conformably overlies the lithic-rich tuff and lapilli tuff lithofacies. It consists of two facies: the crystal- and pumice-rich tuff facies that is locally and conformably overlain by the stratified facies (Table A1; Fig. A4B, C).

The crystal- and pumice-rich tuff facies is massive and contains strongly clay altered, elongate and wispy quartz and K-feldspar porphyritic, long-tube pumice clasts that are supported by a clay-altered groundmass containing crystals and crystals shards (Fig. A4B). Overall, the crystal- and pumice-rich tuff facies has a rhyolitic composition. The stratified facies is restricted to one outcrop and consists of well-stratified and cross-stratified, crystal-rich tuff (Table A1). Columnar joints, oriented perpendicular to bedding, occur throughout the entire preserved thickness of the crystal-rich pumice tuff lithofacies (Table A1; Fig. A4C).

The lenticular and wispy shape of the flattened pumice clasts within the crystal- and pumice-rich tuff facies are characteristics of fiamme, and their parallel orientation defines a pronounced eutaxitic texture that is interpreted to have formed during welding and compaction (Fisher and Schmincke, 1984; Cas and Wright, 1987; McPhie et al., 1993; Branney and Kokelaar, 2002). These features plus the development of columnar joints are indicative of hot deposition and along with the crystal-rich matrix are typical of Lower and Upper Volcanic Succession ignimbrites (Aguirre-Díaz and McDowell, 1991; Swanson et al., 2006; Ferrari et al., 2007). The sedimentary and volcanic clasts within the crystal- and pumice-rich welded facies are identical to clasts within the underlying lithic-rich tuff and lapilli tuff lithofacies (Table A1).

The planar and cross-stratified crystal-rich beds of the stratified facies are characteristic of pyroclastic surge deposits (Fisher and Schmincke, 1984; Cas and Wright, 1987). The occurrence of columnar joints throughout the stratified facies indicates incipient welding and the restriction of this facies to one outcrop suggests significant erosion of the stratified facies along with total removal of an overlying, coeval, hot pyroclastic deposit(s); the latter is required to account for the incipient welding and development of columnar joints throughout

the entire exposure of the stratified facies. Thus, the crystal-rich pumice tuff lithofacies and perhaps, the underlying lithic-rich tuff and lapilli tuff lithofacies mark an abrupt change from a below storm wave base marine environment that existed during deposition of the Pitarrilla formation to a subaerial environment at the time of ignimbritic volcanism that was followed by a period of erosion. This change from a submarine to a subaerial environment, followed by a period of extensive erosion, required uplift within the eastern flank of the central sector of the Sierra Madre Occidental.

Stratified tuff lithofacies: The stratified tuff lithofacies, including a basal lapillistone facies that is divisible into a monolithic and a heterolithic lapillistone, conformably overlies the crystal-rich pumice tuff lithofacies (Table A1). The stratified tuff lithofacies consists of well-sorted planar beds containing angular, millimeter-sized clasts and crystal fragments (Table A1; Fig. A4D).

The stratified tuff lithofacies displays features that are consistent with deposits formed from the upper dilute part of high-density turbidity currents characterized by suspension and traction sedimentation (Lowe, 1982; Allen et al., 2007). This interpretation implies that the La Pitarrilla area returned to a subaqueous environment, either lacustrine or marine, following erosion of the underlying crystal-rich pumice tuff lithofacies.

Lithic-rich tuff lithofacies: The lithic-rich tuff lithofacies conformably overlies and is locally interbedded with the stratified tuff lithofacies. The lithic-rich tuff lithofacies contains wispy, elongate, clay- and hematite-altered, aphyric clasts, rounded to angular heterolithic volcanic clasts, and sparse rounded clasts of terrigenous sedimentary rocks within a strongly clay altered matrix (Table A1).

The pronounced similarity of this lithofacies to lithic tuff of the underlying lithic-rich tuff and lapilli tuff lithofacies, which also contains aphyric wispy clasts of possible pumiceous origin, suggests it may represent another ignimbrite deposit. However, the absence of a planar fabric defined by the parallel orientation of wispy (pumiceous) clasts indicates cool deposition with no evidence of heat retention (i.e., incipient welding). Alternatively, the wispy clasts could result from compaction of cold pumice (vitric) clasts during lithification and diagenesis of either primary pyroclastic flow deposits or their redeposited equivalents. The depositional environment is uncertain as characteristics of this lithofacies are consistent with subaerial or subaqueous deposition.

Casas Blancas formation

The Casas Blancas formation unconformably overlies the Cardenas formation and comprises a lower and upper volcanoclastic lithofacies and the overlying Encino rhyolitic dome lithofacies (Table A1; Figs. 2–5).

Lower volcanoclastic lithofacies: The relatively flat-lying lower volcanoclastic lithofacies unconformably overlies tilted strata of the Cardenas formation (Table A1; Figs. 2–5). This volcanoclastic lithofacies contains rounded to angular andesitic and dacitic clasts, with lesser irregularly shaped, aphyric, clay-altered clasts in a fine tuff-sized matrix (Table A1; Fig. A5A).

The depositional environment of this volcanoclastic facies is uncertain as the poor size sorting, the massive nature, and the

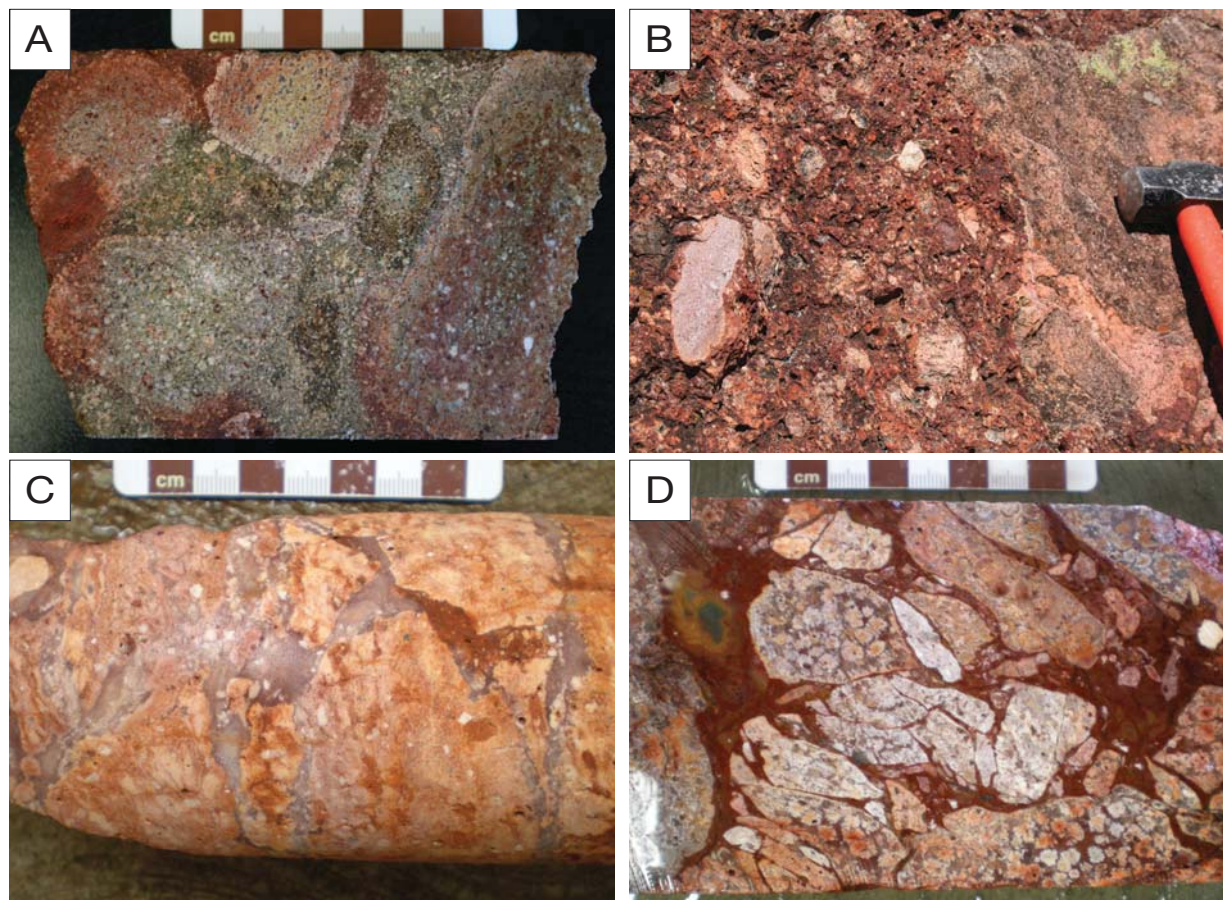


FIG. A5. Members and lithofacies of the Casas Blancas formation. A. Nonbedded and poorly sorted clay- and hematite-altered lower volcaniclastic lithofacies containing rounded to subrounded dacitic and andesitic clasts within a tuff-sized matrix containing abundant feldspar. B. Nonbedded tuff breccia of the upper volcaniclastic lithofacies containing rhyolitic clasts of the overlying Encino rhyolitic dome lithofacies (pink clasts) and rounded to angular volcanic clasts within a tuff-sized matrix. C. Hematite-altered, monomictic rhyolite breccia with a chalcedony matrix (Encino rhyolitic dome lithofacies). D. Hematite-altered hyaloclastite at the basal contact of the Encino rhyolitic dome lithofacies.

matrix-supported character of the lower volcaniclastic lithofacies are consistent with both subaerial and subaqueous deposits.

Upper volcaniclastic lithofacies: The upper volcaniclastic lithofacies is restricted to the base of the overlying Encino rhyolitic dome lithofacies where it conformably overlies the lower volcaniclastic lithofacies (Table A1; Figs. 2–5). It is similar to the latter but differs in that it contains abundant, subrounded to angular, commonly flow-banded rhyolite clasts that are identical to the overlying Encino rhyolitic dome lithofacies (Table A1; Fig. A5B). The upper volcaniclastic lithofacies is divisible into two facies, based on differences in bed thickness and clast size: a medium to thickly bedded tuff and lapillistone facies at the base overlain by a nonbedded lapillistone to tuff breccia facies (Fig. A5B).

The poor sorting with respect to clast size and composition and the dominantly massive nature of the upper volcaniclastic lithofacies are characteristics of both subaerial and subaqueous volcaniclastic deposits. The restriction of the upper volcaniclastic lithofacies to the base of the Encino rhyolitic dome suggests that it could be a product of mass wasting of fault scarp walls. Alternatively, the andesitic and dacitic clasts could be sourced from outside of La Pitarrilla and deposited

within localized basins. In either scenario, the rhyolitic clasts, some more than a meter in size, are interpreted to have been derived through mass wasting of a growing and advancing Encino rhyolitic dome.

Encino rhyolitic dome lithofacies: The Encino rhyolitic dome lithofacies conformably overlies the upper volcaniclastic lithofacies (Figs. 2–5). It has a rhyolitic composition and contains K-feldspar and quartz phenocrysts within a coherent, flow-banded, microcrystalline quartz groundmass (Table A1; Fig. A5C). The basal 3 to 40 m of the Encino rhyolitic dome is marked by perlitic fractures, lithophysae, and spherulites; hyaloclastite occurs locally at the contact with underlying strata (Fig. A5D). In the dome interior, monolithic rhyolitic breccias locally occur over 15- to 40-cm intervals (Fig. A5C). The upper contact of the Encino rhyolitic dome lithofacies has been removed by erosion.

The base of the Encino rhyolitic dome displays hyaloclastite, which implies that at least the base of the dome was emplaced in a subaqueous environment or onto wet and unconsolidated volcaniclastic rocks. Therefore, the two underlying volcaniclastic lithofacies of the Casas Blancas formation, like the Encino rhyolitic dome, may have been emplaced into

a localized lacustrine or a marine environment. Flow banding, spherulites, perlitic texture, columnar joints, and hyaloclastite can occur in rhyolitic sills, cryptodomes, and domes. The only evidence to support an extrusive emplacement is the occurrence of Encino rhyolitic dome clasts within the upper volcanoclastic lithofacies. However, the upper contact of the Encino rhyolitic dome is not preserved and the extrusive interpretation is tentative. The restriction of the Encino rhyolitic dome to an area delimited by the vertically projected traces of older faults and lobe orientations that broadly parallel the orientation of the two main fault sets suggests emplacement of the Encino dome within a fault-controlled, topographic basin.

Intrusions

Mafic sills: A lower mafic sill occurs within the Lower and Middle members of the Pitarrilla formation and is laterally continuous in drill cores across La Pitarrilla (Figs. 2–5). An upper mafic sill occurs within the upper volcanoclastic lithofacies of the Casas Blancas formation. It is restricted in its areal extent and is preferentially oriented in a north-northwest-south-southeast direction that is parallel to the north-northwest-trending fault set (Fig. 3).

The lower mafic sill is green or mauve in color due to chlorite and hematite alteration. It consists of a coherent massive facies that has at its lower and upper margins a peperite facies (Fig. A6A, B). The coherent massive facies has an andesitic composition and contains amphibole phenocrysts within a microcrystalline plagioclase groundmass (Table A1; Fig. A6A). An in situ breccia occurs locally at the transition between the coherent massive facies and the upper and lower peperite facies. The in situ breccia consists of angular clasts of the lower mafic sill with jigsaw-fit texture that grades inward into the coherent massive facies and outward into peperite; the latter typically contains irregularly shaped clasts of the lower mafic sill mixed within the enveloping volcanoclastic lithofacies (Fig. A6B). The upper mafic sill also has an andesitic composition and contains amphibole phenocrysts, replaced by opaque minerals and epidote, within a microcrystalline groundmass dominated by plagioclase (Table A1). The upper mafic sill, like the lower mafic sill, varies in color between green and mauve, depending on alteration. The upper mafic sill has peperite within its interior, consisting of irregularly shaped clasts of the upper mafic sill enclosed within the upper volcanoclastic lithofacies. On a primitive mantle normalized multielement plot, the lower and upper mafic sills display

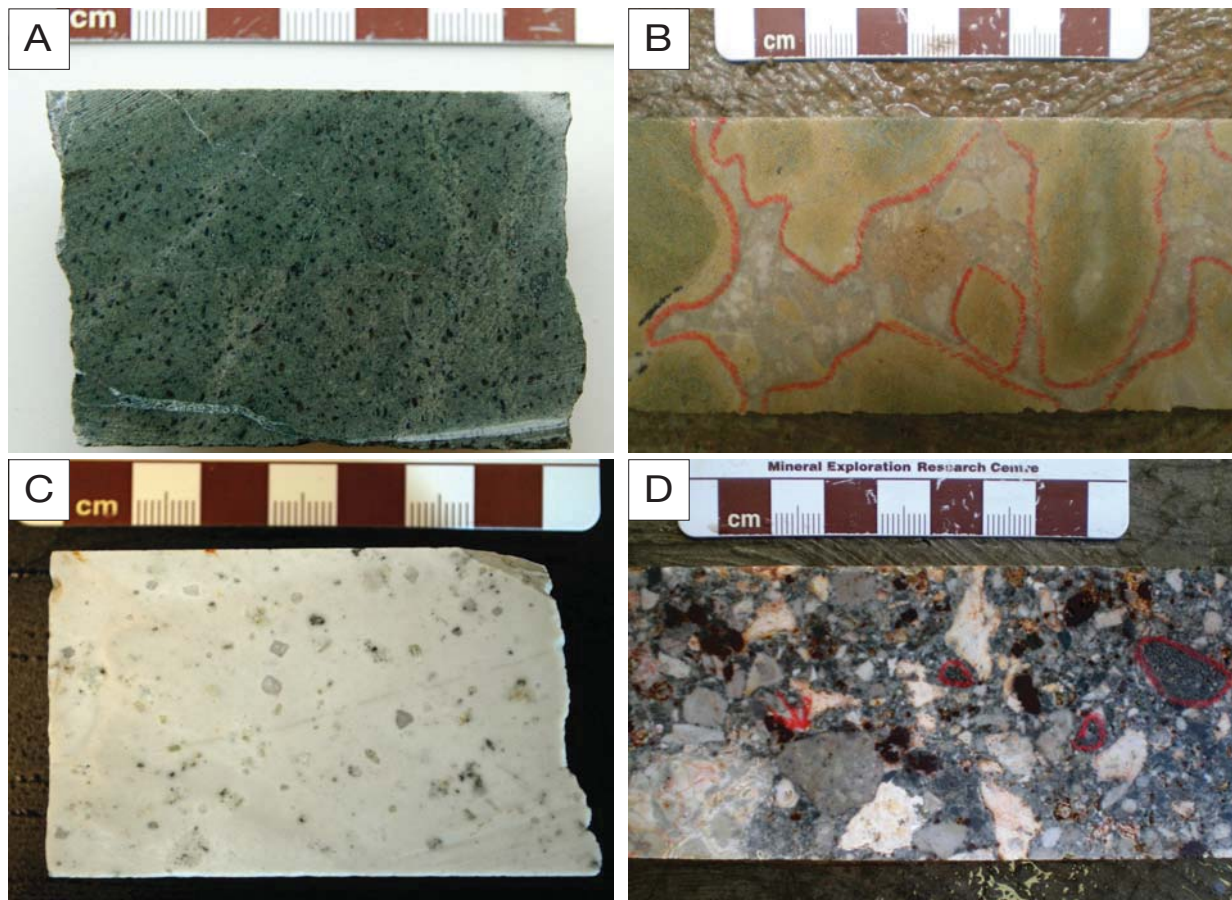


FIG. A6. Intrusions. A. Chlorite-altered, coherent facies of the lower mafic sill with chlorite altered mafic crystals. B. Chlorite- and iron carbonate-altered peperite facies of the lower mafic sill that consists of irregularly shaped clasts of the lower mafic sill mixed with volcanoclastics of the Pitarrilla formation. C. Quartz-porphyritic felsic dike. D. Peperite facies of a felsic dike that is composed of irregularly shaped clasts of the felsic dike mixed with tourmaline-altered Pitarrilla formation volcanoclastic rocks.

negative Nb, Ta, and Ti anomalies, and moderately steep REE patterns, which are indicative of arc volcanism (Fig. A3D).

The occurrence of peperite along the contacts of the lower mafic sill and within the upper mafic sill indicates that they are intrusions (e.g., White et al., 2000) and that the volcanoclastic deposits of the Pitarrilla and Casas Blancas formations were still unconsolidated and wet at the time of sill emplacement. This is consistent with the interpretation for a marine environment during emplacement of the Pitarrilla and Casas Blancas formations. As the lower mafic sill does not appear to be significantly displaced by the two main fault sets that offset the Cardenas formation, its emplacement is interpreted to be pre-Encino rhyolitic dome emplacement as the felsic dikes that are the feeders for the Encino dome crosscut the lower mafic sill (Figs. 3–5). The occurrence of the upper mafic sill within the upper volcanoclastic lithofacies, which contains blocks of the Encino rhyolitic dome, indicates that it was emplaced during or just after emplacement and growth of the Encino dome. This implies that the upper mafic sill is younger than the lower mafic sill and that volcanism was bimodal (andesite-rhyolite).

Felsic intrusions: Felsic dikes crosscut all strata at La Pitarrilla except the Encino rhyolitic dome, whereas felsic sills occur only within the Pitarrilla formation (Figs. 2, 4, 5). The felsic dikes and sills are concentrated and converge at the highest elevation of La Pitarrilla where the Encino rhyolitic dome occurs (Figs. 3–5). The felsic dikes have two preferred orientations, which are the northeast-southwest and north-northwest-south-southeast orientations that parallel to the orientation of the northeast- and north-northwest-trending fault sets (Fig. 3). The felsic intrusions consist of a coherent facies and locally a peperite facies (Table A1; Fig. A6C, D).

The dikes and sills are rhyolitic in composition and contain K-feldspar and quartz phenocrysts within a microcrystalline quartz groundmass (Fig. A6C). On primitive mantle normalized diagrams, the felsic intrusions display negative Eu and Ti anomalies, a LREE enrichment, and have a flat HREE pattern that is not typical of arc rhyolites (Fig. A3E). Peperite occurs locally for 10s of centimeters to 10s of meters along the margins of the coherent facies, and especially where the dikes cut volcanoclastic lithofacies of the Pitarrilla, Casas Blancas, and more rarely, Peña Ranch formations. Peperite consists of irregular, delicate to fluidal-shaped clasts of quartz and feldspar porphyritic rhyolite within a volcanoclastic matrix (Fig. A6D).

The occurrence of peperite along the margins of felsic dikes emplaced within the Pitarrilla and Casas Blancas formations is consistent with their emplacement into wet, unconsolidated volcanoclastic rocks (e.g., White et al., 2000), and supports a subaqueous environment during the emplacement of these formations. The jigsaw-fit texture and evidence of clast rotation indicates that the breccia facies was mainly formed in situ. The identical mineralogy, composition, textures, and structures of the felsic intrusions and the Encino rhyolitic dome, as well as their gradation upward into the Encino dome, indicate that they are the feeders for the Encino dome. Therefore, the area where the felsic dikes converge in Figures 4 and 5 is interpreted to define the primary vent area for the Encino rhyolitic dome, which is now preserved as two flow lobes within eroded fault-bounded basins adjacent to its feeding fissure. The parallel trend of the felsic dikes and the two faults sets suggests that these early faults, or ancillary parallel structures, were reactivated during Casas Blancas volcanism where they acted as structural conduits for felsic magmas.